ADVANCING EARTH AND SPACE SCIENCES

Tectonics

RESEARCH ARTICLE
10.1029/2024TC008463

Key Points:

- Interpretation of high-quality 3D seismic data unraveled the detailed structural setting of the easternmost Jura fold and thrust belt
- Different types of pop-ups and triangle zones are controlled by the style of interaction with sub-décollement structures
- The key transition from thin-skinned thrusting to deep-seated shortening may be documented by the analyzed seismic volume

Correspondence to:
S. Mazzoli,
stefano.mazzoli@unicam.it

Citation:
Zambrano, M., Mazzoli, S., Mosar, J., & Pedini, M. (2025). Modes of deformation in sedimentary multilayers interacting with sub-décollement structures: Insights from 3D seismic interpretation in the eastern Jura fold and thrust belt. *Tectonics*, *44*, e2024TC008463. https://doi.org/10.1029/2024TC008463

Received 12 JUN 2024
Accepted 7 JAN 2025

Author Contributions:
Conceptualization: S. Mazzoli, J. Mosar
Data curation: M. Zambrano, M. Pedini
Formal analysis: M. Zambrano, M. Pedini
Funding acquisition: S. Mazzoli
Investigation: M. Zambrano, S. Mazzoli, J. Mosar
Methodology: M. Zambrano, M. Pedini
Project administration: S. Mazzoli
Resources: S. Mazzoli
Software: M. Zambrano, M. Pedini
Supervision: S. Mazzoli, J. Mosar
Validation: M. Zambrano, S. Mazzoli, M. Pedini
Visualization: M. Zambrano, M. Pedini
Writing – original draft: M. Zambrano, S. Mazzoli
Writing – review & editing: S. Mazzoli, J. Mosar

Modes of Deformation in Sedimentary Multilayers Interacting With Sub-Décollement Structures: Insights From 3D Seismic Interpretation in the Eastern Jura Fold and Thrust Belt

M. Zambrano[1], S. Mazzoli[1], J. Mosar[2], and M. Pedini[1]

[1]School of Science and Technology, Geology Division, University of Camerino, Camerino, Italy, [2]Department of Geosciences, University of Fribourg, Fribourg, Switzerland

Abstract The Jura fold and thrust belt is characterized by dominant thin-skinned thrusting and variable interaction with inherited structures and deep-seated (i.e., sub-décollement) faults. Using 3D seismic data, the styles of deformation and the relationships with inherited structures at the eastern termination of the fold and thrust belt are documented in an area located NW of the city of Zürich. The investigated seismic volume includes two major, ENE trending fold-thrust zones involving the Triassic-Jurassic epicontinental platform succession and the stratigraphically overlying Cenozoic Molasse Basin deposits. The location of both fold-thrust zones appears to be controlled by variable interaction between the décollement level hosted in the Triassic evaporites of the Muschelkalk Group and faults linked to an underlying Permian-Carboniferous graben. Different modes of interaction of the Mesozoic multilayer (including the weak evaporite level close to its base) and underlying upper Paleozoic basin fill with inherited faults produced a marked contrast in structural style (pop-up and triangle zone geometry) between the N and S fold-thrust zones. We suggest that the different types of structures provide an unprecedented record of the transition from thin-skinned thrusting (dominant in the N fold-thrust zone) to deeply rooted deformation controlled by the inherited structural architecture of the upper Paleozoic basin. Such a transition was characterized by focusing of strain from the upper Paleozoic section to a narrow belt of Mesozoic strata, triggering coeval buckling and reverse faulting (manifested in the S fold-thrust zone). Propagation of sub-décollement faults and segment linkage eventually led to breaching of the regional detachment.

Plain Language Summary Following extensive geological, geophysical, and drilling campaigns, an overconsolidated Jurassic shale (the Opalinus Clay, dated at ca. 175 Ma) was selected by Swiss authorities to host a deep geological repository in the Nördlich Lägern site. A high-quality data set including deep well logs and a 3D seismic volume was used to study subsurface geology of this site. Our interpretation provides an unprecedented record of the modes of transition between two fundamental deformation styles in fold and thrust belts, from detachment-dominated thrusting of the sedimentary cover to basin inversion associated with bulk crustal shortening. Although the Jura Mountains are considered a paradigmatic example of the switch between these two different deformation styles, previous studies were never able to document such a transition with the level of detail allowed by the exceptional data set made available to us.

1. Introduction

Pop-ups and various types of triangle zones are well known structural features in fold and thrust belts (e.g., Barnes & Nicol, 2004; Butler, 1982; von Hagke & Malz, 2018, and references therein). The development of such structures is controlled by a series of parameters including décollement occurrence and type, competence contrasts in multi-layered rocks, occurrence and role of inherited structures, dominant deformation mechanisms—and hence P, T, fluid pressure conditions—and thrust/fold propagation/growth rates (e.g., Costa & Vendeville, 2002; Coward et al., 1999; Davis et al., 1983; Fabbi & Smeraglia, 2019; Watkins et al., 2017). Extensive analogue and numerical modeling indicate that increasing friction along the basal décollement facilitates the development of doubly faulted anticlines (simple pop-ups; Figures 1a–1c) or more complex structural assemblages including several forethrusts and backthrusts (termed here composite pop-ups; Figures 1d and 1e) (e.g., Graveleau et al., 2012). Simple pop-ups range from doubly faulted anticlines sitting in the hanging wall of a thrust and a backthrust branching from the frontal ramp of the former (Figure 1a), to doubly faulted box folds

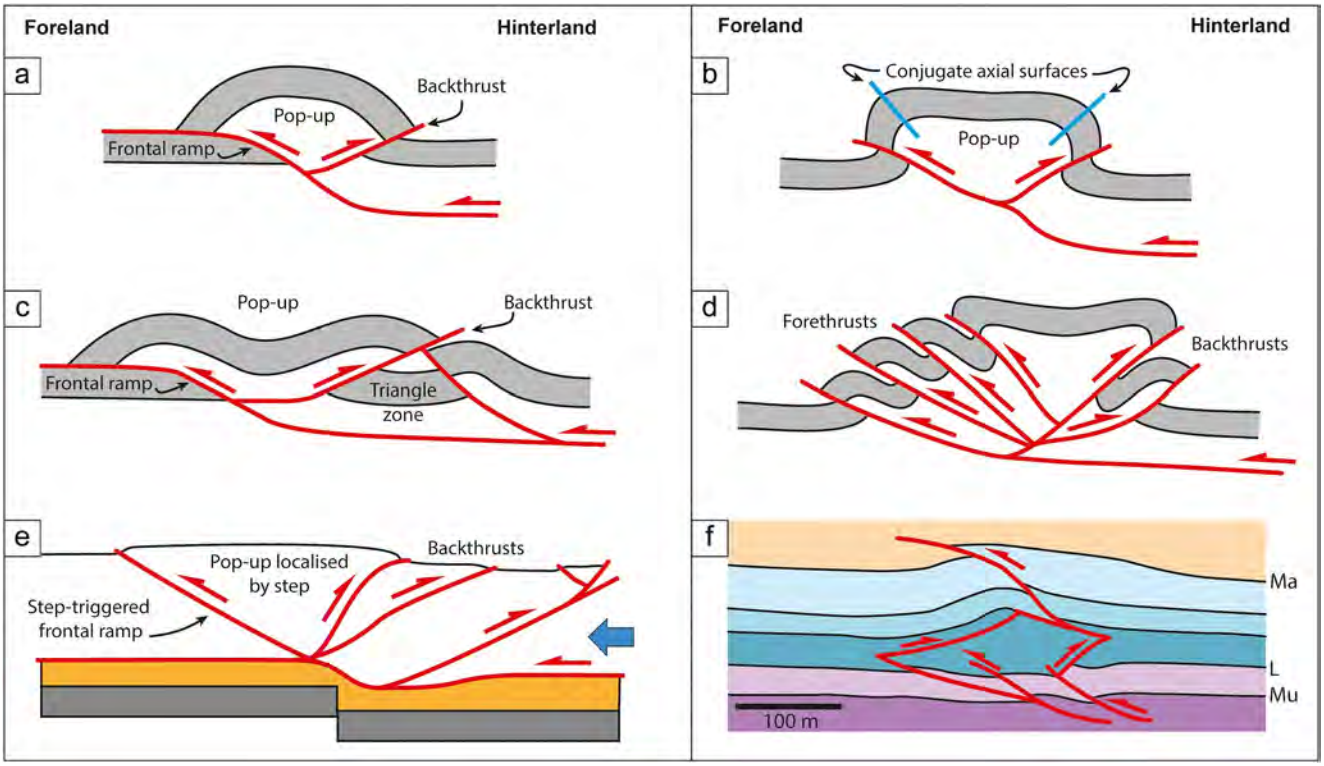

Figure 1. Types of pop-ups and triangle zones discussed in this study. (a) Simple pop-up developed in the hanging wall of a backthrust branching out from a frontal thrust ramp. (b) Simple pop-up consisting of doubly faulted box fold. (c) Simple pop-up consisting of paired anticlines and central syncline, and adjacent triangle zone (after Butler, 1982). (d) Composite pop-up including more numerous foreland-directed thrust splays. (e) Sketch summarizing the results of analogue modeling by Schori et al. (2021) showing composite pop-up (including more numerous hinterland-directed thrust splays) developed above a weak décollement level (orange) at a substratum step (dark gray). Blue arrow shows the direction of push. (f) Seismic interpretation (after Laubscher, 1986) from the area of the present study, showing fishtail structures. Triangle zones developed in this instance are of intercutaneous wedge type (McClay, 1992). Mu = top Middle Triassic (Muschelkalk); L = top Lower Jurassic (Lias); Ma = top Jurassic (Malm).

characterized by conjugate, oppositely dipping axial surfaces and a flat crestal region (Figure 1b), to anticline pairs separated by a central syncline in the hanging wall of a thrust-backthrust pair (Figure 1c). Composite pop-ups, dominated by hinterland-dipping thrust splays (Figure 1d) or foreland-dipping backthrusts (Figure 1e), may form at sites of interaction between the décollement and basement steps (Schori et al., 2021). These latter are well known to represent "décollement obstacles" controlling thrust ramp nucleation in the Jura fold and thrust belt (Laubscher, 1986). On the other hand, vertically superposed sets of hinterland- and foreland-dipping reverse faults forming multiple tectonic wedges, known as fishtail structures (Figure 1f), accommodate layer-parallel shortening in multi-layered rocks, including in the Jura fold and thrust belt (Laubscher, 1986). Thickness ratio and mechanical contrast among layers as well as the distance from the main décollement are important features in governing the formation and geometry of such fishtail structures (Jaquet et al., 2014).

Based on the structural interpretation of a 3D seismic volume (Nördlich Lägern) located at the eastern termination of the Jura fold and thrust belt (Figure 2), this study investigates the geological settings leading to the development of the different types of deformation features described above. Following extensive geological, geophysical, and drilling campaigns (https://nagra.ch/en/product-category/technical-reports/), the overconsolidated Aalenian Opalinus Clay, dated at ca. 175 Ma; (Zimmerli et al., 2024) was proposed by the Swiss National Cooperative for the Disposal of Radioactive Waste (Nagra) to host a deep geological repository in the Nördlich Lägern site (Figure 3).

The eastern termination of the Jura fold and thrust belt is characterized by a marked decrease in deformation and tectonic transport, associated with a change in the amount of salt and other evaporites hosting the main décollement level. The area of investigation is located at the transition from a clearly contractional tectonic regime (Jura fold and thrust belt) to an extensional setting at the fringes of the Bodensee-Hegau Graben system (e.g., Egli et al., 2016; Madritsch et al., 2024; Malz et al., 2016). The occurrence of an important Permian-Carboniferous

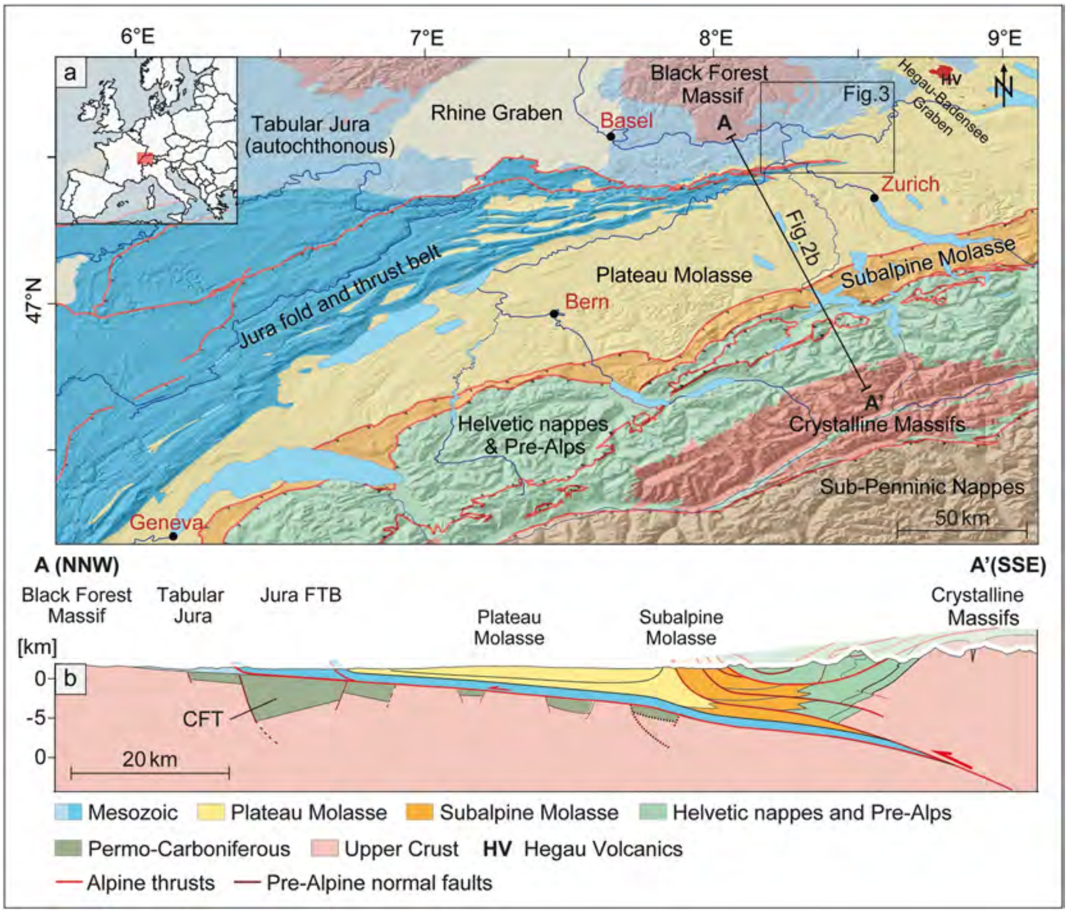

Figure 2. Tectonic sketch map (a) and regional cross-section A-A′ (b) of the eastern Jura Mts. and surrounding Alpine-Molasse Basin-European foreland region (modified after Looser et al., 2021). The map shows the position of the Rhine Graben and Black Forest, and location of the map in Figure 3. CFT = Constance-Frick Trough.

graben system resulted in considerable substratum topography and inherited faults that, upon reactivation, produced substratum steps variably affecting the main décollement level. Since the décollement level is underlain by upper Paleozoic sedimentary units—and not crystalline basement, we prefer to refer to the general concept of "substratum" rather than basement for the steps associated with deep faults in the study area. Our objective is to highlight the different tectonic styles associated with variable degrees of substratum-cover interaction, as recorded in the deformed Meso-Cenozoic succession. A competition and combination of thin-skinned thrusting and thick-skinned (i.e., basement-involved) deformation can be expected, as the Jura fold and thrust belt represents a paradigmatic example of the switch from detachment-dominated thrusting and folding of the sedimentary cover (Buxtorf, 1916) to bulk crustal shortening in the outer zone of collisional orogens (Balansa et al., 2022; Giamboni et al., 2004; Lacombe & Bellhasen, 2016; Lacombe & Mouthereau, 2002; Madritsch et al., 2008; Malz et al., 2016; Meyer et al., 1994; Mosar, 1999; Philippe et al., 1996; Pfiffner et al., 1997; Rotstein & Schaming, 2004; Schöpfer et al., 2024; Ustaszewski & Schmid, 2006, 2007). However, the modes by which such a transition occurs have never been investigated with the level of detail provided by the exceptional 3D data set used in this study. The implications of our interpretation have a profound impact on the comprehension of the regional tectonic evolution and, more in general, on the understanding of the modes of interaction between substratum and cover series in fold and thrust belts.

2. Geological Setting

The Jura fold and thrust belt (Figure 2) is part of the detached Alpine foreland, together with the Molasse Basin. Whereas the Jura is composed of Triassic to Cretaceous epicontinental, carbonate-rich strata, the Molasse Basin is

10.1029/2024TC008463

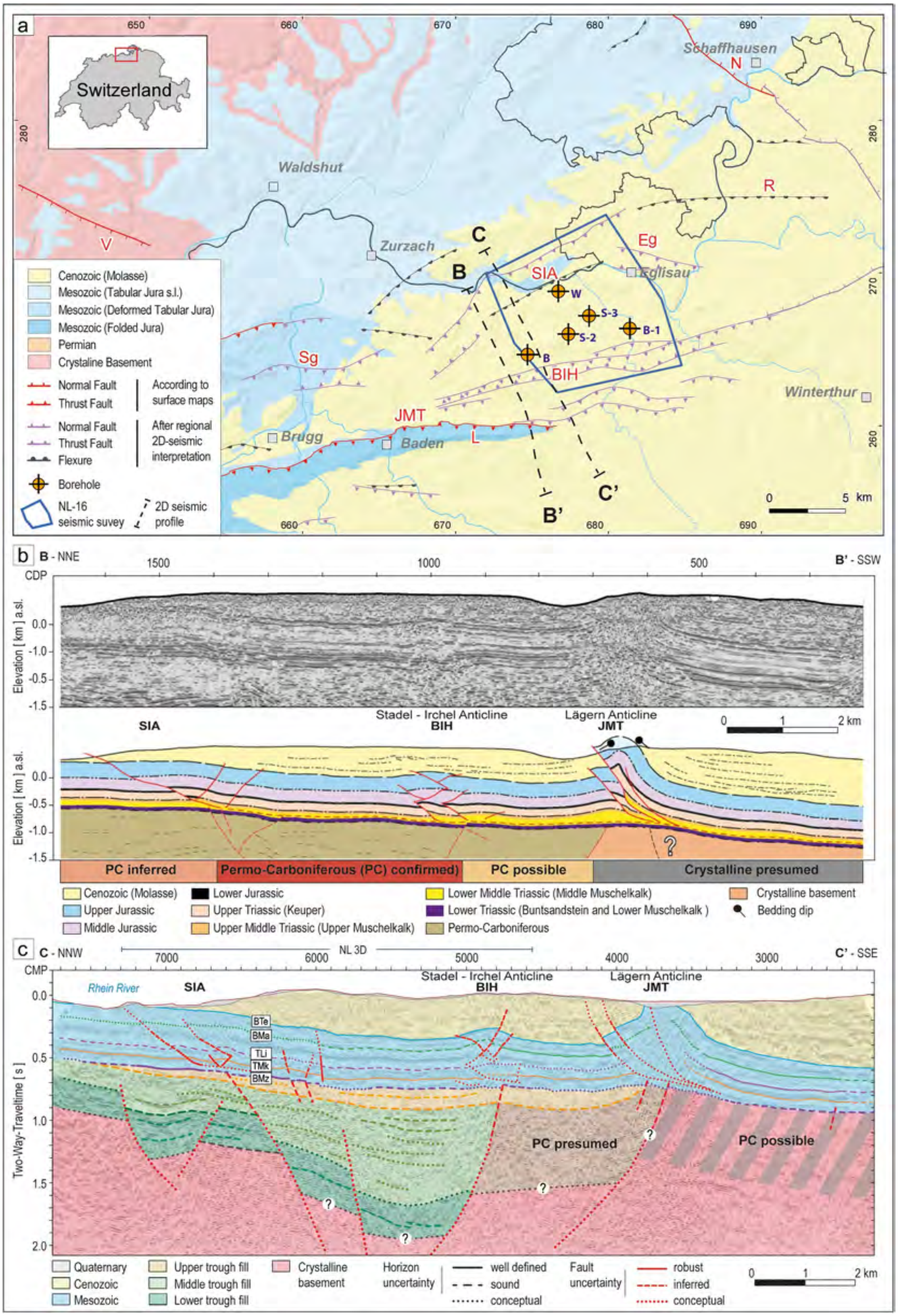

Figure 3.

characterized mostly by Cenozoic sediments linked to the formation and erosion of the Alps. The Molasse Basin initiated as a flexural foreland trough in Eocene times. In Early Middle Miocene times it evolved to a detached and transported wedge-top basin as the Jura fold and thrust belt started to develop (e.g., Becker, 2000). These processes were controlled by the presence of major décollement levels in the Middle and Upper Triassic salt-rich evaporite series (Muschelkalk and Keuper Groups; Jordan, 1992). Lower Triassic sandstones lie beneath the main décollement and therefore are part of the mechanical substratum.

Within the study area (Figure 3), the main décollement level is constituted by the evaporite units of the Zeglingen Fm (Figure 4). U-Pb ages from syntectonic calcite veins from the study area have been related with thrusting between 14.3 and 4.5 Ma (Looser et al., 2021), thus roughly aligning with prior stratigraphy-based estimates (Becker, 2000, and references therein). More recent radiometric ages obtained by the same method have been interpreted in terms of detachment-dominated thrusting from ca. 12 to ca. 8 Ma, followed by further shortening till ca. 4 Ma (Madritsch et al., 2024). The field observations linking the U-Pb ages to structural development in the study area are not conclusive with respect to the nature—detachment-dominated or more deeply rooted—of the later deformation, which may have produced fold tightening according to the authors.

The Nördlich Lärgern area is located north of the Lägern anticline, which is the easternmost thrust-related fold of the Jura belt and is classically associated with the Jura Main Thrust (Jordan et al., 2015; Figure 3b). As such, the Lägern anticline is part of the Internal Jura (Haute-Chaîne). North of if, our study area belongs to the External Jura (Plateau Jura), which is formed by alternating narrow antiformal belts ("Faisceaux") and wide synformal areas ("Plateaux"; Swisstopo, 2005). Immediately N of the Lägern anticline, a gentle anticline occurs at the surface. This gentle antiform is characterized by fishtail structures in the subsurface (Baden-Irchel-Herdern triangle zone in Malz et al., 2016). Beneath the main décollement level, major N-dipping normal faults define the southern border of the Permian-Carboniferous graben known as Constance-Frick Trough (Madritsch et al., 2018, and references therein; Figure 3c). The major fault underlying the Lägern anticline represents an inherited ENE-striking basement feature (fault step with basement topography) that was shown to concentrate deformation and to influence the structural style of the overriding Jura fold and thrust belt (Caër et al., 2018). North of it, shortening of the Mesozoic succession occurred along the western segment of the so-called Baden-Irchel-Herdern (BIH) triangle zone (also controlled at depth by an upper Paleozoic fault; Malz et al., 2016), while farther to the east the whole succession up to the base of the Cenozoic shows an extensional offset along the same lineament (Egli et al., 2016; Malz et al., 2016). The area north of the BIH triangle zone lies on top of the main upper Paleozoic graben system, whose sedimentary fill and underlying basement were penetrated for ca. 1,500 m by the Weiach deep borehole (located in Figure 3). The drilled Paleozoic succession consists of 456.4 m of Lower to Middle Permian beds and 572.6 m of Upper Carboniferous (Stephanian) beds unconformably overlying crystalline basement (Schöpfer et al., 2024, and references therein). The upper Paleozoic, heterogeneous continental succession includes two stratigraphic units separated by an unconformity (Intra-Permian Unconformity; Jordan & Deplazes, 2019). The upper unit (Weitenau Formation, 262 m thick) consists of alluvial fan deposits made of arkose sandstones and fanglomerates, and subordinate littoral sediments including siltstones and sandstones. The lower unit (not formally defined, 767 m thick) consists of fine- to coarse-grained sandstones, siltstones and claystones. The Carboniferous section also includes an interval of ca. 200 m (from 1,551 to 1,752 m below the topographic surface) of coal seams that are up to few meters thick and embedded in a partly bituminous and heterolithic succession of claystones, siltstones and sandstones (Nagra, 2014).

Besides the main ENE-striking graben edge faults, major NW-striking structures also occur (e.g., the Eglisau fault in Figure 3). These are well documented structures that extend beyond the graben system into the outcropping pre-Mesozoic basement in the Black Forest area, also controlling the original segmentation of the upper Paleozoic extensional fault system (Madritsch et al., 2018). Along the NW edge of the studied seismic volume, the Siglistorf Anticline forms the outermost deformation feature in the study area.

Figure 3. Overview of the tectonic setting of northern Switzerland based on previous studies. (a) Simplified tectonic map (modified after Nagra, 2019) showing location of the Nördlich Lägern (NL) seismic volume at the transition between the detached and autochthonous foreland basin (folded and tabular Jura, respectively) and profiles B-B′ and C-C′. Fault traces after the regional 2D-seismic interpretation represent the tip lines of faults at top Mesozoic level. JMT = Jura Main Thrust; BIH = Baden-Irchel-Herdern triangle zone; Eg = Eglisau fault; SIA = Siglistorf Anticline. Wells in the study area: W = Weiach, S-2 = Stadel-2, S-3 = Stadel-3, B-1 = Bulach-1, B = Bachs-1; (b) Depth-converted 2D regional seismic line and related geological section (modified after Malz et al., 2016). (c) Interpreted 2D regional seismic line (modified after Madritsch et al., 2018). BMz = Base Mesozoic; TMk = Top Muschelkalk (Middle Triassic); Tli = Top Lias (Lower Jurassic); BMa = Base Malm (Upper Jurassic); BTe: Base Tertiary (Cenozoic).

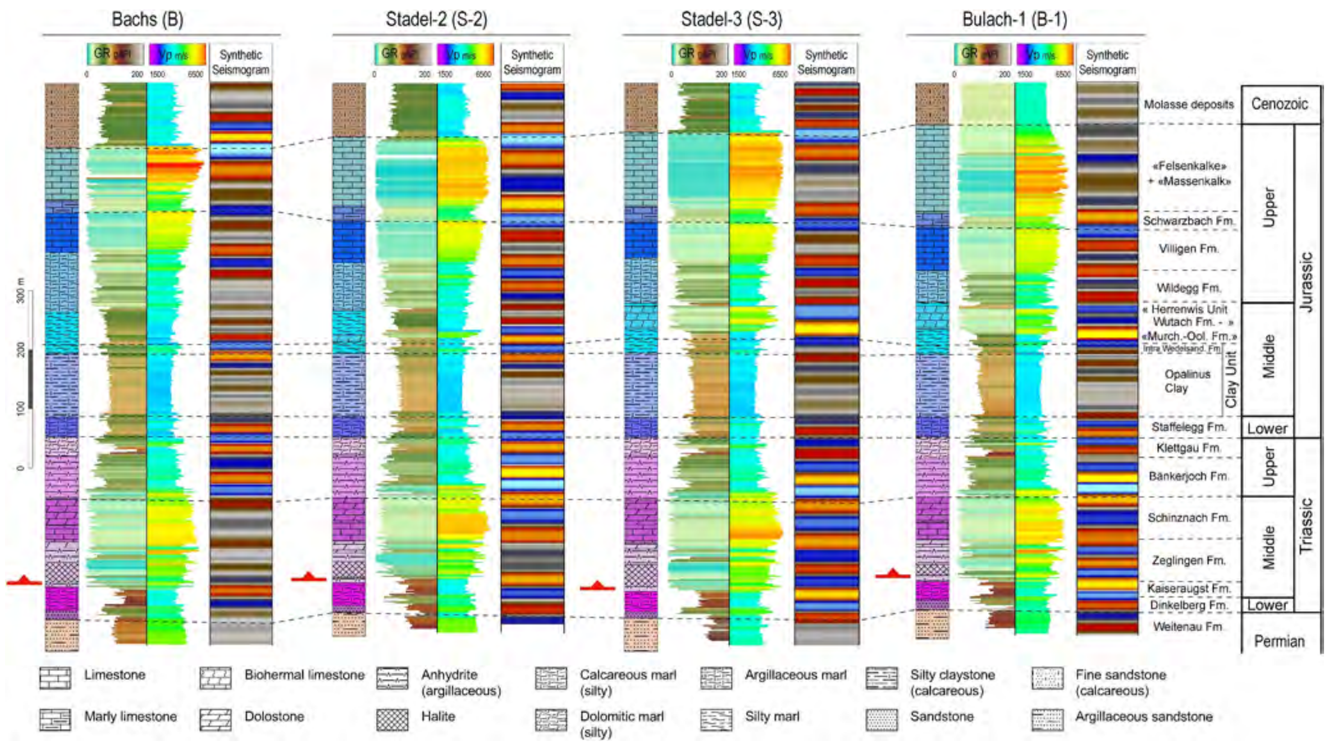

Figure 4. Well correlation diagram including stratigraphic columns for the Meso-Cenozoic succession and well log data (provided by Nagra) from four boreholes within the study area. Red lines with triangles show the location of the main décollement.

In addition to the inherited substratum topography, deformation of the Mesozoic-Cenozoic sedimentary cover is strongly controlled by the presence and distribution (thickness; Adams & Diamond, 2019) of salt in the Muschelkalk Group evaporites. It was proposed that below a threshold thickness value of around 150 m the décollement is no longer active (Sommaruga et al., 2017). This would place our study area in a critical setting with respect to detachment-dominated thrusting, considering Muschelkalk halite and total evaporite thickness shown in Figure 4. In synthesis, the area of investigation is located at the NE edge of the Jura fold and thrust belt, in a region where the décollement tapers out and where basement-involved deformation—including the reactivation of inherited faults—may have occurred (Schöpfer et al., 2024). The main inherited structures are linked to pre-existing Permian-Carboniferous graben faults (shoulder-parallel and oblique). However, further extensional faulting/fault reactivation is associated with both Paleogene flexure of the foreland plate and development of the Oligocene Rhine Graben rift (which is part of the European Cenozoic Rift System; e.g., Laubscher, 1986).

3. Materials and Methods

3.1. Data Set

This study is based on the use of 3D seismic data and the integration with key wells drilled by the Nationale Genossenschaft für die Lagerung radioaktiver Abfälle (NAGRA). The 3D seismic survey Nördlich Lägern (NL) was acquired in 2016. It covers an area of ~91 km^2, with NNW-SSE trending inlines having a line spacing of 15 m. NAGRA has generated and facilitated for academic research different versions corresponding to different processing workflows according to the objectives or phase of the studies in the area (Eichkitz et al., 2020). The version used in this study is characterized by a zero phase, a normal—according to the convention adopted by the Society of Exploration Geophysicists (SEG) for the display of zero-phase seismic data—standard polarity and a mean frequency varying from 45 Hz for the Mesozoic to 30 Hz in the Permian succession. In addition, NAGRA provided a Pre-Stack-depth migration velocity cube. Well log data consist of formational or geological age tops, gamma ray, density, porosity, sonic, caliper, and vertical seismic profile–(VSP) from five boreholes located within the study area (Weiach, Stadel-2, Stadel-3, Bulach-1, and Bachs-1), which allowed calibration. The whole data set was loaded into Petrel software (Schlumberger) for data integration and interactive interpretation. The

Petrel project was set up using a seismic reference datum of 650 m, a replacement velocity of 3,500 m/s and an X/Y coordinate system identical to that of the Swiss Reference System CH1903. Original, uninterpreted seismic data used in this study are available in Zambrano et al. (2024; https://doi.org/10.6084/m9.figshare.26021614).

3.2. Seismic-Well Calibration

A first step in seismic interpretation consists in relating the seismic and well data, which are in two-way-time and depth domain, respectively. To do this, seismic-well tie was carried out by a synthetic seismograms calibration methodology (Simm & Bacon, 2014) included: (a) quality control and edition of log removing spikes and filling gaps, (b) Time Depth Relationship (TDR) estimation from the VSPs data set (or sonic for the Weiach well), and (c) wavelet extraction from the seismic data at borehole location using a statistical approach for the convolution. The wavelet amplitude spectrum is directly derived from scanning of seismic traces at intervals of interest. Phase is assumed to be constant and equal to zero. Seismic-to-well ties were performed by using the Time Depth Relationship derived by sonic logs calibrated with VSP data and statistical Ricker wavelet extraction (courtesy of Nagra). Only a bulk shift was performed, avoiding ad hoc stretches. Synthetic seismograms show an interval characterized by a poor impedance contrast related to a Clay Unit that includes the Opalinus Clay and surrounding argillaceous-marly strata from the top of the Stafelegg Fm to the basal member of the Herrenwies Unit (Figure 4). Multiples (artifacts) were identified within the Opalinus Clay interval. The acoustic properties of the Opalinus Clay do not support the observed relatively high-amplitude reflectivity pattern. Separation between primary and secondary seismic patterns is therefore extremely challenging, hampering interpretation in this stratigraphic interval.

3.3. Fault and Horizon Interpretation Strategy

A structural interpretation following main reflectors and discontinuities associated with faults was focused on both the Mesozoic-Cenozoic succession and pre-Mesozoic units. We focused on the following characteristics: (a) reflector/horizon geometry; (b) horizon continuity and presence of interruption/discontinuities; (c) horizon cut-offs; and (d) evaluation of additional structures such as folds, bumps etc.

In the case of horizon interpretation, a standard approach was applied combining semi-automatic 2D-tracking and 3D-tracking for expanding the interpretation, following the same phase in most of the cases, except for unconformities. The identified main reflectors were interpreted in the areas with higher coherency, avoiding unclear zones where moderate noise affected the propagation of the 2D semi-automatic interpretation. These areas were covered in a second round by manual picking and/or interpolation. The interpretation followed a seedline square approach: starting from wells, a narrowing down strategy was applied from an initial 32×32 interval to a final 8×8 interpretation grid. To check inconsistencies in the interpretation and to implement surface attributes in further steps, the Petrel autotrack algorithm was used to fill gaps between the 8×8 interpreted grid. This uses the 8×8 grid as seedpoints, thus preserving the original interpretation. Parameters include a correlation of 0.8, a 3×3 expansion coefficient, and 30% amplitude confidence. The autotracked horizons undergo both automatic and manual checks for errors and inconsistencies. Following this strategy, the tracking of horizons was also a guide for fault identification. Some limitations arose in the areas where the horizon segments superposed ("multi-z") due to the presence of reverse faults; in such instances, the uppermost segment of the horizon was kept, while the footwall segment (truncated vertically beneath the hanging-wall cutoff by the interpretation software) was reconstructed by generating a brother horizon segment reaching the footwall cutoff and filling the empty space of the "multi-z."

Fault interpretation was implemented into two phases: reconnaissance and 3D mapping. The first was aimed at defining main areas of deformation and structural styles, and to find alignments associated with discontinuities of the seismic data by means of 3D variance attribute (which is an edge-method measuring the similarity of waveforms or adjacent traces in vertical or horizontal seismic profiles, thereby highlighting discontinuities in seismic data) and edge detector on 3D horizons. In this phase, a distinction was made among seismic discontinuities related with structural elements and stratigraphic features, seismic noise, and artifacts (acquisition footprints and overburden geology imprints). The second phase was focused on 3D interpretation of the architecture of faults and the detailed structural modeling of the area of interest. A clear offset of reflectors, identified for more than 120 m (eight seismic lines), was used as a secondary indicator of faults with smaller offsets. Near the detection limits of the seismic data, we relied on seismic discontinuities identified by the variance attribute. This was used in conjunction with variations in reflector geometry (reflection deflection) affecting multiple stratigraphic levels and indicating fault-related structures, seismic character variation, or fault-plane reflections (mostly from low angle faults). The combination of these techniques helped us to extend fault identification near their tip, where fault throw approaches the resolution limits, or in the areas where reflector offsets are difficult to observe or identified in a single line. Similar to the interpretation of horizons, a narrowing down strategy was followed by manually interpreting fault sticks up to eight lines (120 m), and in particular cases every four lines (60 m) for solving subtle or complex geometry. Larger faults were mapped first, thereby creating a structural framework of primary structural features, followed by an infill interpretation including smaller structures. The geometry of single fault segments and the architecture of fault arrays was also verified by observing multiple orientation sections, attribute maps, and 3D visualization. Viewing the faults in 3D space by simultaneously correlating attribute time/horizon slices and vertical sections enhances the 3D geometrical understanding of the structure, guiding segment interpretation, and highlights segment shape and position inconsistencies.

3.4. Cross-Section Balancing

To build a balanced geological section along a representative inline of the seismic data set, interpreted horizons and faults were converted to depth using the available smoothed Pre-Stack Depth Migration velocity cube. Subsequently, minor adjustments were applied to the converted surfaces to improve the alignment with well-tops. The process ensures that the seismic horizons and faults are geologically consistent with borehole data, resulting in a more reliable final geological section. This was imported into Move software (Petroleum Experts) for balancing and restoration. This well-established procedure is based on the assumptions of no volume change and plane strain (of course with the plane of the section being parallel to the plane of bidimensional strain). In these conditions, the shortening estimated by area balancing includes the internal strain of the rocks, which cannot be accounted for by simple line-length balancing. Structural analysis of drill cores indicates that, besides structures that are consistent with the regional NNW shortening direction (parallel to our balanced section), a component of NNE shortening is also recorded at the core scale (Decker et al., 2022). This is consistent with the results of regional structural work carried out by Madritsch (2015). Therefore, the plane strain assumption is not satisfied in our study area. However, the moderate angular difference between the two shortening directions and the consistent ENE trend of Jura fold-thrust structures imply that the amount of missing finite strain is likely minor in our restoration. Concerning the assumption of no volume change, it may be envisaged that it is essentially satisfied as: (a) less competent lithologies of the Mesozoic succession, including the Clay Unit, consist of silty claystones and argillaceous-marly strata that were certainly well lithified prior to Neogene deformation, and are therefore unlikely to have experienced substantial lateral compaction (Butler & Paton, 2010) associated with horizontal shortening; and (b) the amount of material dissolved by pressure-solution processes dominant in calcareous lithologies is likely to be roughly balanced at the section scale by the amount of material (essentially calcite; Madritsch et al., 2024) precipitated in nearby or surrounding veins, thus resulting in overall volume preservation—and area conservation in 2D—as a result of dissolution-precipitation creep.

The balanced cross-section was restored to the pre-thrusting stage by the application of the 2D Move-on-Fault tool for the thrusts. We anticipate that the analyzed structural assemblages are dominated by blind reverse faults and zones of tectonic thickening around fault tips, as well as layer thickness variations in the folded Mesozoic multilayer. 2D modeling of these structures involved accounting for the deformation of areas comprised within a triangular zone of shear by applying the appropriately designed Trishear algorithm (Erslev, 1991). This method involves area preservation within the triangular zone of shear emanating from the tip of a propagation fault, while deformation of the hanging wall block outside such a zone is modeled by the Fault Parallel Flow algorithm (Egan et al., 1999); tuning of various geometrical parameters allows one to define the shape and location of the trishear zone. Unfolding was carried out using the 2D Unfolding tool operating with the Line Length method. Both line-length and area balancing were then performed on the data obtained from the 2D Section Analysis tool. This tool automatically restores line lengths by removing fault offsets and correcting for folding effects. To obtain a pre-deformational template of geological units that can be used in shortening calculations by area balancing, stratigraphic thicknesses were measured along four pin lines perpendicular to bedding placed in macroscopically undeformed areas. In order to take into account the apparently slight (see below) original stratigraphic thickness variations characterizing the study area, average thicknesses were calculated between each pair of adjacent pin lines. These values were then compared with the average thickness of each unfolded stratigraphic unit calculated by the software (using either vertical or bisector measurements) to check their consistency. The cumulative initial thickness values obtained by the two methods differ by a maximum of 45 m (i.e., 5%). On the other hand, the estimated initial cumulative thickness of the Mesozoic succession used in shortening calculations varies along the section by a maximum of 78 m (i.e., 9%), thereby almost approaching a simple layer-cake stratigraphy.

The previously mentioned structural analysis of well cores by Decker et al. (2022) shows that even the apparently undeformed zones of the study area are affected by distributed layer-parallel shortening strain. As such zones unaffected by seismic-scale deformation are those controlling the calculation of original stratigraphic thicknesses, the shortening values obtained by area balancing must be considered as minimum estimates. However, this is probably an issue common to most fold and thrust belts, as regionally "undeformed" rock panels that are used to measure original stratigraphic thicknesses are commonly affected by some layer-parallel shortening (and related thickening, in case of plane strain and no volume change; e.g., Groshong et al., 2012). Roughly unchanged stratigraphic thicknesses could perhaps be obtained from undeformed foreland areas, but then there could be substantial lateral variations of original thicknesses of the formations with respect to those involved in the fold and thrust belt. Stratigraphic correlations assuming constant thicknesses of the formations over large distances may introduce an even larger degree of uncertainty (e.g., Butler, 1989) with respect to that characterizing the relatively small and stratigraphically homogeneous area of this study (refer to the well logs in Figure 4).

4. Results

The main structural trends identified at the level of the Mesozoic units include ENE- and NW-striking structures (Figure 5). The investigated seismic volume includes two major, ENE trending fold-thrust zones involving the Triassic-Jurassic epicontinental platform succession and the stratigraphically overlying Cenozoic Molasse Basin deposits. The northern fold-thrust zone is known as the Siglistorf Anticline (SIA), whereas the southern one is called Baden-Irchel-Herdern (BIH) triangle zone. The fold-thrust zones are consistently located above steep faults imaged in the underlying Permian-Carboniferous Constance-Frick Trough (Figure 6a). The fold-thrust zones are characterized by highly non-cylindrical structures and intense fault segmentation, both along strike and along the vertical direction (Figures 6b and 7). Between the northern and the southern fold-thrust zones, a tectonic feature known as Weiach-Glattfelden-Eglisau Lineament (WGEL) overlies a major fault of the upper Paleozoic Constance-Frick Trough (CFT). The lineament is best detected in variance attribute maps, and it is defined by high angle faults showing minor (<10 ms) vertical separation. The central area between the BIH triangle zone and the WGEL is characterized by a homoclinal rock panel, termed here Bachs-Bülach Homocline (BBH). This homoclinal rock panel is located over the area characterized by the largest thickness of the Paleozoic succession in the main depocenter of the CFT. The BBH area is also characterized by an absence of alignments in variance attribute maps (Figure 5), as well as a constant thickness of the Opalinus Clay (Figure 4).

4.1. N Fold-Thrust Zone

The N fold-thrust zone, manifested at the surface by the Siglistorf Anticline, consists of a composite pop-up including highly segmented thrust and backthrust splays. The substratum step observed in the seismic volume is associated with south-dipping faults of the CFT graben; (Figure 6). The composite pop-up forming the N fold-thrust zone is up to 2 km wide. Its internal architecture is characterized by an elevated along-strike variability, involving lateral changes from faulted folds with rounded hinge zones to faulted box folds and kink bands (Figure 8). The Clay Unit is locally thickened around the tip zones of thrust and backthrust splays that remain blind within this unit, as they do not offset the Top Clay Unit. On the other hand, the Top Clay Unit is locally offset by reverse faults that appear not to be connected with those cutting across the base of the unit (see uppermost backthrust in Figure 8a). These features suggest that strain is ductilely accommodated within the incompetent Clay Unit, in which soft linkage of fault segments may also occur.

4.2. S Fold-Thrust Zone

The S fold-thrust zone is located above a fault system controlling the southern sector of the CFT graben (Figure 6). This fold-thrust zone consists of multiple hinterland- and foreland-dipping reverse faults, and related triangle zones of intercutaneous wedge type (McClay, 1992) forming a series of fish-tail structures arranged in a several hundred meters wide, steep belt involving the Triassic-Jurassic strata (Figure 9a). Malz et al. (2016) calculated a shortening of ∼200 m across the S fold-thrust zone, this value remaining essentially constant along

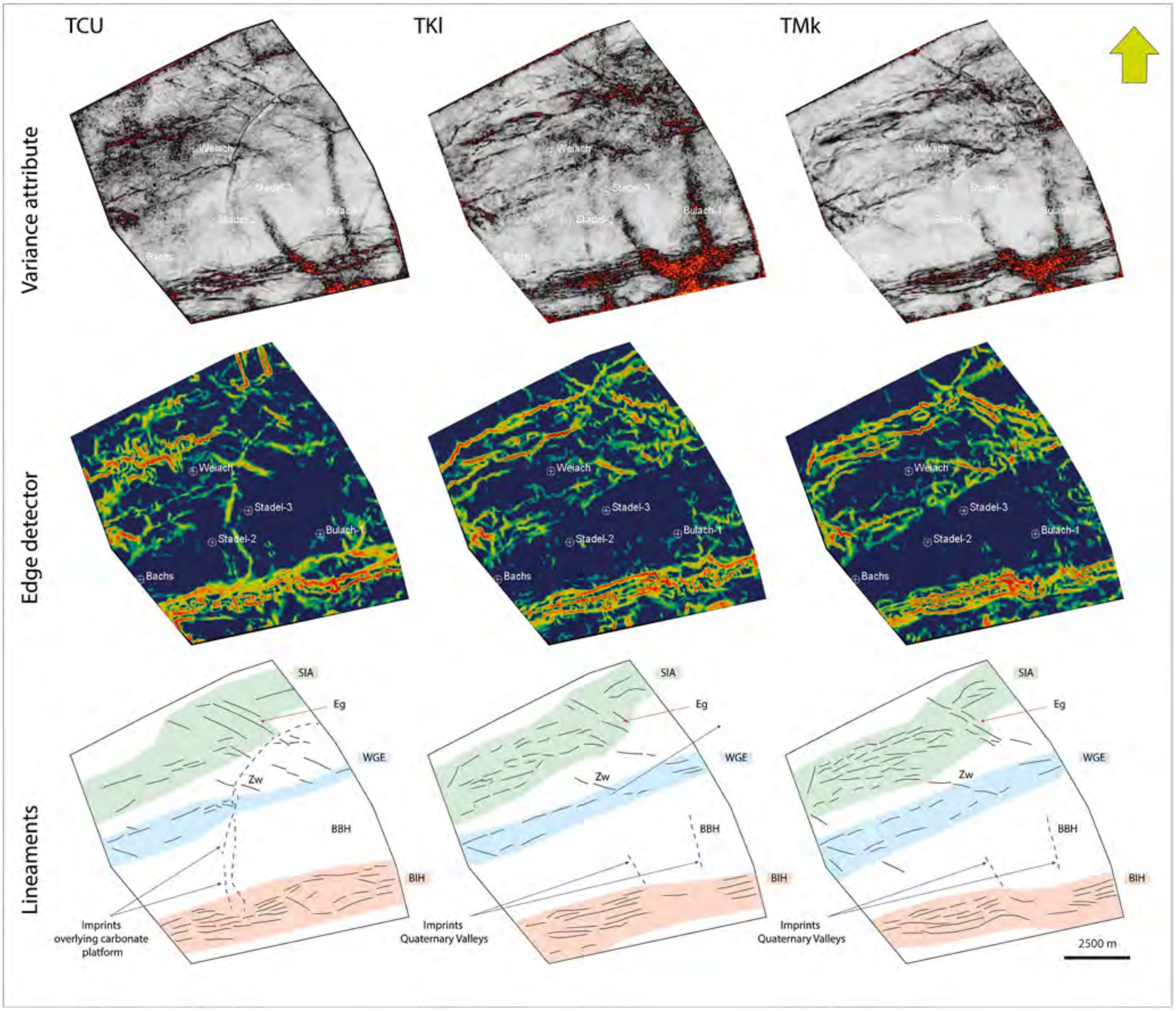

Figure 5. Results of the reconnaissance phase emphasizing lineament identification and key deformation zones. Variance attribute, edge detector results, and lineaments (highlighting various features—including imprints of overlying carbonate platform and Quaternary valleys—besides fault traces) maps for three critical horizons: Top Clay Unit (TCU; reflector 168.2_Baj_400 in seismic data; left column), Top Klettgau (TKl; central column), and Top Muschelkalk (TMk; left column). BIH = Baden-Irchel-Herdern triangle zone; BBH = Bach-Bulach Homocline; WGEL = Weiach-Glattfelden-Eglisau Lineament; Zw = Zweideln fault; Eg = Eglisau fault; SIA = Siglistorf Anticline.

strike west of our study area. The incompetent Clay Unit appears to have allowed decoupling of the deformation between a lower competent panel (thick-bedded to massive limestones and dolostones of the Upper Muschelkalk) and an upper competent panel consisting of thick-bedded to massive limestones of the Villigen Fm and Upper Malm. The clayey rocks, that are characterized by a rather constant original (i.e., stratigraphic) thickness over the whole study area of Figure 3a (Zimmerli et al., 2024), are imaged as shortened and mechanically thickened between the two disharmonically folded, competent rock panels located above and below them (Figure 9a). Reverse fault splays offset the Base Mesozoic Unconformity as well as the décollement level hosted in the Triassic evaporites of the Muschelkalk Group. The continuity of reverse fault splays into the stratigraphic units overlying the Base Mesozoic Unconformity is more marked at an oblique ramp sector of the S fold-thrust zone (Figure 9b).

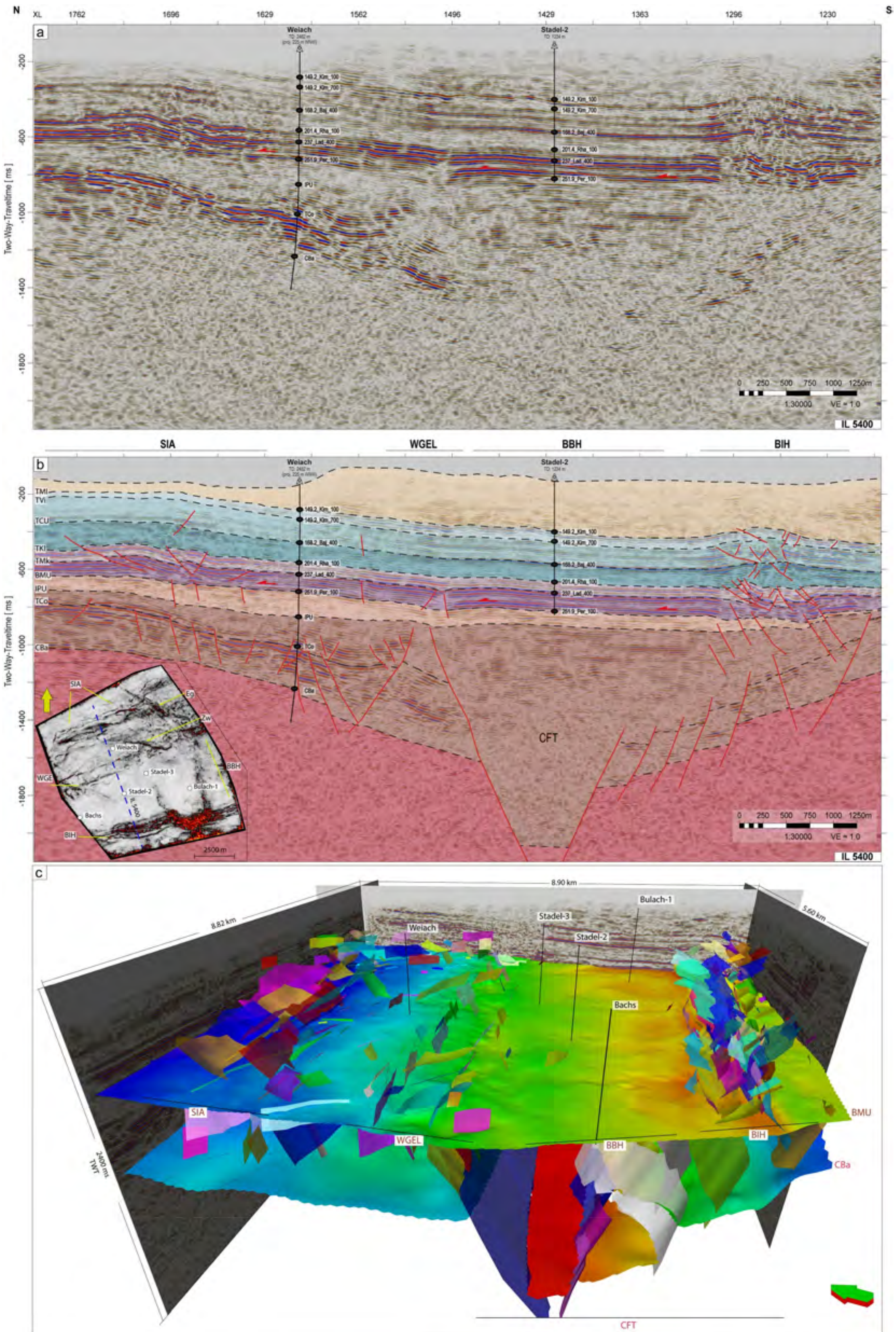
N
S
a
b
c
SIA
WGEL
BBH
BIH
Weiach
Stadel-2
Stadel-3
Bulach-1
Bachs
Two-Way-Traveltime [ms]
IL 5400
CFT
BMU
CBa
8.90 km
8.82 km
5.60 km

Figure 6.

4.3. High-Angle Faults

High-angle faults offsetting the Mesozoic succession in the NL seismic volume are arranged along the previously mentioned dominant trends (ENE and NW) that also affect the underlying Paleozoic units. Most of these faults offset the lower part of the Mesozoic succession and are not seismically imaged within the Clay Unit (Figure 10). Several faults are observed in the succession overlying the Clay Unit, which appears to have acted as a decoupling level for deformation also for these steep faults. Only a few, larger faults offsetting the Triassic-Lower Jurassic formations show upward continuity through the Clay Unit and overlying stratigraphic units (Figures 5 and 7).

Faults mapped below the Base Mesozoic Unconformity show either normal (Figure 8) or reverse (Figure 9) dip-slip components of motion. The former characterizes deep faults involving the basement, while the latter are common within the Permian-Carboniferous basin fill (from which they may often be traced into the overlying Mesozoic succession; Figure 10). Faults showing a reverse dip-slip component of motion may have propagated from the inherited upper Paleozoic faults, however they mostly appear as newly formed splays that developed in their proximity (Figures 9 and 10). These faults offset the near base Mesozoic unconformity. Because of their reverse dip-slip components, they are referred to Neogene shortening (probably postdating detachment-dominated thrusting, as they offset the evaporite décollement level). These moderately to steeply dipping reverse faults may also have a modest (i.e., not larger than the dip-slip separation and not often clearly identifiable on seismic data) strike-slip component of motion, in that case representing oblique-slip structures.

Roughly in the middle of the seismic volume, the ENE-striking Weiach-Glattfelden-Eglisau Lineament (WGEL) forms a major fault system imaged by seismic data (Figure 10). The WGEL, including faults offsetting the Base Mesozoic Unconformity, appears to represent a hinge zone between two regional rock panels (N and S of it) showing different angles of dip. A sub-horizontal to gently folded Mesozoic rock panel occurs to the south, while a gently S-dipping panel occurs to the north. Thickness changes in the Permian-Carboniferous succession indicate a syn-sedimentary, extensional/transtensional late Paleozoic origin for the deeper fault segments controlling the WGEL. Later, shortening-related—probably oblique-slip—fault reactivation/propagation/nucleation along the WGEL may have accompanied minor tilting of the previously described rock panels during Neogene crustal shortening.

In the central-northern part of the NL seismic volume, the NW striking Zweideln and Eglisau faults produced a marked compartmentalization of the N fold-thrust zone. The Zweideln fault also separates two different segments of the WGEL at the level of the Mesozoic units (Figures 5 and 7).

4.4. Balanced Cross-Section

The depth-converted interpretation of the seismic profile of Figure 6a generated the cross-section shown in Figure 11. Line-length and area balancing were carried out for the whole cross-section and separately for three sectors (from N to S): (a) N fold-thrust zone, (b) central zone (including the WGEL), and (c) S fold-thrust zone. The stratigraphic markers considered in cross-section balancing were the following (from base to top): Intra-Permian Unconformity (IPU), Base Mesozoic Unconformity (BMU), Top Muschelkalk (TMk), Top Klettgau (TKl), Top Clay Unit (TCU), Top Villingen (Tvi), and Top Malm (TMl). The relevant data are listed in Tables 1 and 2. The different shortening values obtained by line-length balancing of individual marker horizons is interpreted as resulting from variable partitioning of the deformation between folding and internal strain (mostly producing layer thickening that appears to be rather substantial in the more intensely deformed zones of the section; Figure 11). In this context, meaningful results in terms of total shortening are furnished by area balancing. Mean total shortening obtained by area balancing of the whole section amounts to 589 m (5.9%). Of this, an amount of 280 m is accommodated by thin-skinned thrusting of the detached Mesozoic-Cenozoic succession at the N fold-thrust zone, while an amount of 218 m is associated with folding and conjugate reverse faulting (fishtail

Figure 6. Overview of the seismic interpretation of the NL seismic volume. (a) Inline 5400. (b) Interpreted inline 5400, showing the main structural elements and the interpreted reflectors tied to the wells Weiach and Stadel-2. Note graben geometry of the upper Paleozoic Constance-Frick Trough (CFT) underlying the Mesozoic-Cenozoic multilayer. Inset: variance attribute map at Top Muschelkalk level, showing structural trends related to the fold-thrust zones and tectonic lineaments. (b) View of interpreted 3D volume showing Base Mesozoic Unconformity and Top Basement horizon, together with fault surfaces. SIA = Siglistorf Anticline; WGEL = Weiach-Glattfelden-Eglisau Lineament; BBH = Bach-Bulach Homocline; BIH = Baden-Irchel-Herdern triangle zone; TMl = Top Malm; TVi = Top Villingen; TCU = Top Clay Unit (168.2_Baj_400); TKl = Top Klettgau; TMk = Top Muschelkalk; BMU = Base Mesozoic Unconformity; IPU = Intra-Permian Unconformity; Tco = Top Coal series; Cba = Top Crystalline Basement.

Figure 7. Vertical sections (inlines; IL) through the 3D seismic volume, showing east (upper left) to west (lower right diagram) development of structures. The spacing between adjacent sections is variable (in the range of 210–1,590 m; for reference, the IL spacing is 15 m). Top Muschelkalk surface with overlying variance attribute obtained by seismic interpretation is also shown.

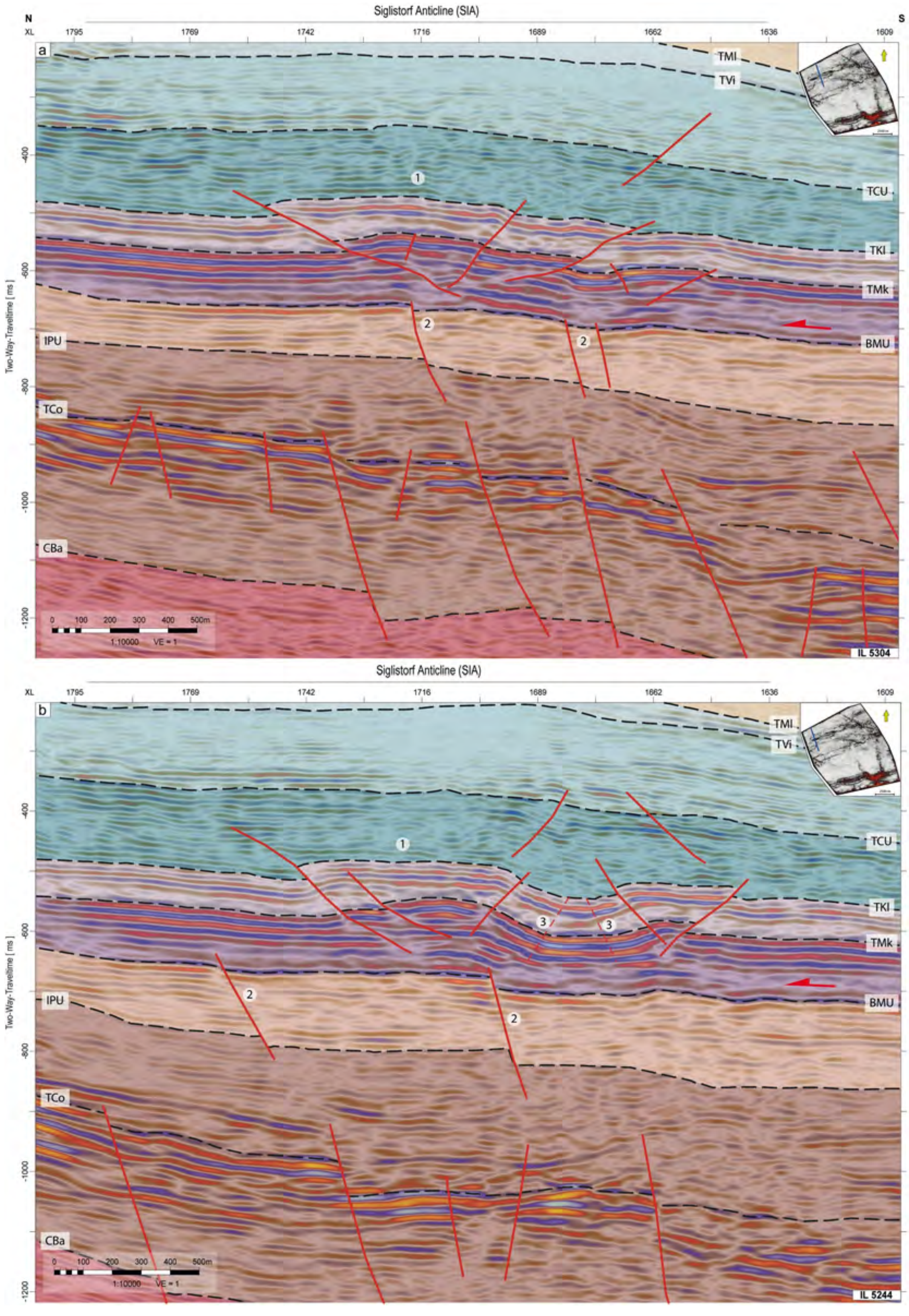

Figure 8. Seismic profiles from the NL seismic volume showing the N fold-thrust zone developed at a substratum step. 1: composite pop-up; 2: substratum steps associated with faults in the Permian-Carboniferous succession; 3: kink bands. Red arrows indicate the approximate location of the décollement level. (a) Inline 5304. (b) Inline 5244. TMl = Top Malm; Tvi = Top Villingen; TCU = Top Clay Unit; TKl = Top Klettgau; TMk = Top Muschelkalk; BMU = Base Mesozoic Unconformity; IPU = Intra-Permian Unconformity; Tco = Top Coal series; Cba = Top Crystalline Basement.

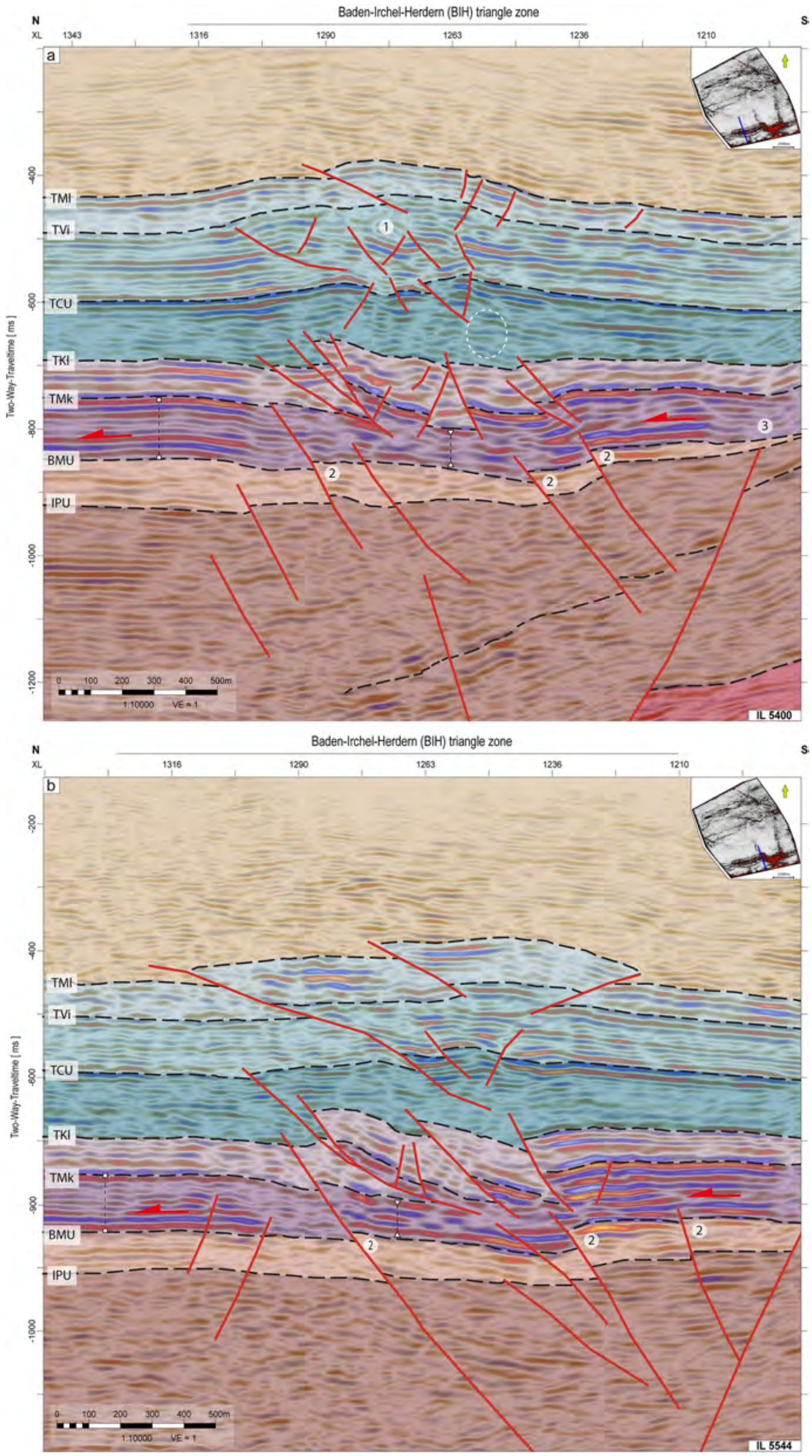
Baden-Irchel-Herdern (BIH) triangle zone
N
S
XL
1343
1316
1290
1263
1236
1210
a
TMl
TVi
TCU
TKl
TMk
BMU
IPU
Two-Way-Traveltime [ms]
400
600
800
1000
1200
0 100 200 300 400 500m
1:10000 VE = 1
IL 5400
Baden-Irchel-Herdern (BIH) triangle zone
b
200
400
600
800
1000
IL 5544

Figure 9.

structures) at the S fold-thrust zone. For this latter, shortening of the Intra-Permian and Base Mesozoic unconformities (obtained by the line-length method) essentially balances that of the overlying Mesozoic multilayer. A further amount of shortening of 91 m (obtained by area balancing of the central zone) is essentially associated with fault segments at the WGEL.

5. Discussion

5.1. Pre-Thrusting Extensional Faulting and Controls on Neogene Structures

Basement structures and upper Paleozoic faults (of extensional/transtensional origin) may have been reactivated with extensional kinematics during: (a) Triassic-Jurassic extension (e.g., Allenbach, 2001, 2002; Malz et al., 2016, Schöpfer et al., 2024; Ustaszweski & Schmid, 2006; Wetzel et al., 2003), (b) Paleogene extension (forebulge/foreland flexure during foreland basin development and/or Rhine graben development; Laubscher, 1986), and (c) Neogene extension (Malz et al., 2016). Minor normal faulting of the Base Mesozoic Unconformity beneath the N fold-thrust zone (Figure 8) was ascribed by Laubscher (1986) to Paleogene extensional reactivation of inherited normal faults. At least some of the extensional structures offsetting the Base Mesozoic Unconformity could also represent newly formed normal fault segments associated with foreland flexure during Paleogene development of the Molasse Basin. In any case, extensional structures observed within the uppermost Paleozoic section and offsetting the Base Mesozoic Unconformity may be interpreted as soft-linked with underlying—probably extensionally reactivated—normal faults occurring within the lower Paleozoic section (Figure 6a). These blind faults have their upper tips confined within the Muschelkalk evaporites, which are interpreted to have accommodated by distributed strain the minor displacement associated with these structures (as already envisaged by Laubscher, 1986). Pre-thrusting extensional reactivation of inherited normal faults and/or renewed normal faulting controlled the development of substratum steps that interacted with the main décollement level during later thrusting. This represents a fundamental issue in the development of fold-thrust structures within the analyzed rock volume. The décollement interacted not only with ENE striking normal fault steps, but also with NW striking features such as the Zweideln and Eglisau faults (Figures 3 and 6). NW striking, inherited basement faults controlled the original compartmentalization of the extensional fault system at the northern edge of the Permian-Carboniferous graben (also extending to the Black Forest north of it; Madritsch et al., 2018). Therefore, they also controlled the spatial arrangement of the substratum steps produced by the Paleogene extensional reactivation of upper Paleozoic normal faults. Such substratum steps, in turn, controlled thrust ramp nucleation during detachment-dominated thrusting. All this resulted in a marked compartmentalization of the N fold-thrust zone by NW trending lineaments that reflect the inherited structural grain of the basement. A more direct influence of the latter is evident for deeply rooted structures such as the WGEL. At the level of the Mesozoic units, the WGEL is segmented by the Zweideln fault and, more to the west, by a further NW striking fault aligned with the oblique ramp segment of the S fold-thrust zone (see, e.g., Top Muschelkalk variance map in Figure 5). These features are consistent with a Neogene reactivation of NW striking inherited faults in the pre-Mesozoic substratum (likely with dominant strike-slip kinematics). At the level of the Mesozoic succession, this process is interpreted to have controlled segmentation and curvature of the deeply rooted WGEL and S fold-thrust zone, respectively. Normal-fault offsets of the Base Mesozoic Unconformity testify to the occurrence of pre-thrusting substratum steps along the northern sector of the CFT, beneath the N fold-thrust zone (Figures 6 and 8). It may be envisaged that S dipping upper Paleozoic normal faults were preferentially reactivated as extensional structures aiding foreland flexuring during the development of the Molasse Basin, thereby producing pre-thrusting substratum steps in the northern sector of the studied volume. On the other hand, at variance with the interpretation by Malz et al. (2016), we see no involvement of a normal fault in the BIH in the same area they discussed. There is no seismic evidence of normal fault-related offsets/deformation

Figure 9. Seismic profiles from the NL seismic volume showing the Baden-Irchel-Herdern (BIH) triangle zone. Note S dipping reverse faults offsetting the Base Mesozoic Unconformity (BMU). 1: fish-tail structure; 2: reverse faults rooted in the Permian- Carboniferous succession offsetting the substratum and the décollement level; 3: BMU not offset/deformed by (either extensional or contractional) reactivation of the underlying N dipping upper Paleozoic normal fault. (a) Inline 5400, showing thickness variations in Muschelkalk evaporites (marked by black dashed lines) and thickening of the incompetent level represented by the Clay Unit (schematically indicated by white dashed ellipse). (b) Inline 5760, showing more continuous reverse faults from late Paleozoic units through overlying Triassic-Jurassic units at an oblique ramp sector (see location map, upper right corner). Black and white dashed arrows indicate differences in thickness in the Muschelkalk unit likely related to evaporite withdrawal. Red arrows indicate the approximate location of the décollement level. TMl = Top Malm; Tvi = Top Villingen; TCU = Top Clay Unit; TKl = Top Klettgau; TMk = Top Muschelkalk; BMU = Base Mesozoic Unconformity; IPU = Intra-Permian Unconformity; Tco = Top Coal series.

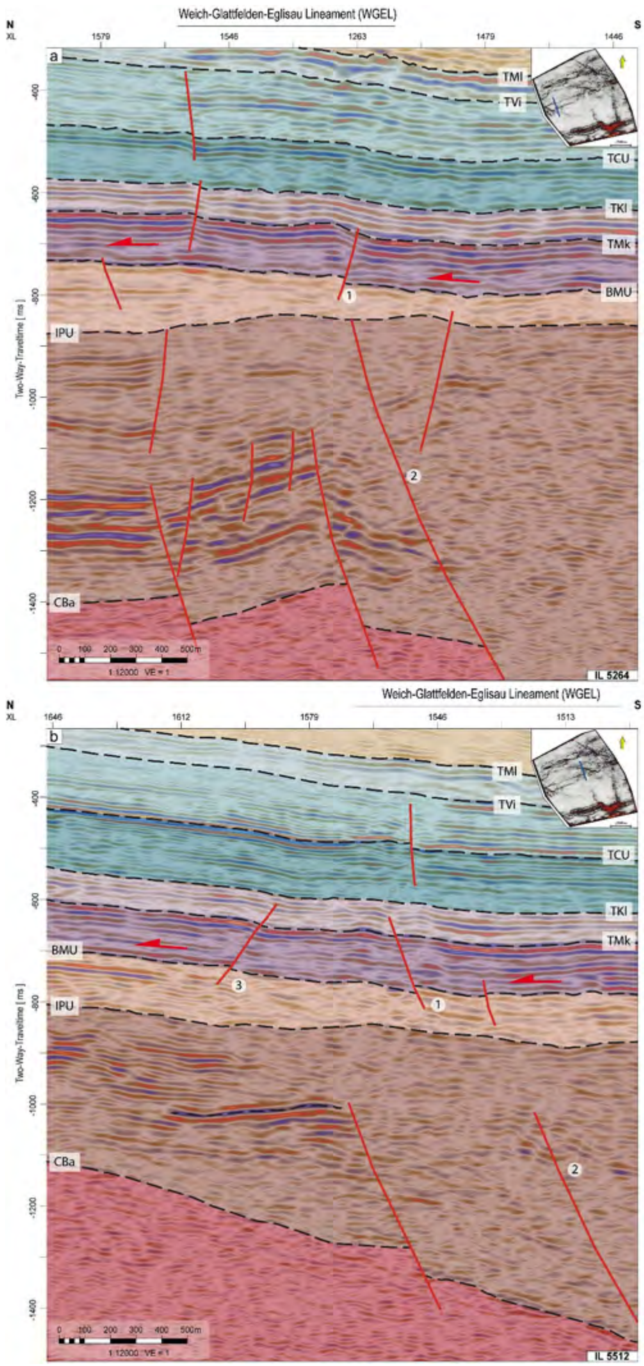

Figure 10. Seismic profiles from the NL seismic volume showing the Weiach-Glattfelden-Eglisau Lineament (WGEL). 1: high-angle faults associated with the WGEL, showing opposite dip directions; 2: faults within the Permian-Carboniferous succession; 3: fault segment associated with the NW striking Zweideln fault. (a) Inline 5264. (b) Inline 5512. Red arrows indicate the approximate location of the décollement level.

of the Base Mesozoic Unconformity in the southern sector of the studied rock volume (Figures 6 and 9). This indicates that N dipping faults of the upper Paleozoic CFT graben were not reactivated at this location during Paleogene foreland flexuring. It must be emphasized that the picture changes dramatically east of our study area, where Jura-related thrusting did not propagate; there, Cenozoic extensional reactivation of basement faults (Roche et al., 2020) also affected the structural trend that controls the southern edge of the upper Paleozoic CFT graben (Egli et al., 2016). This resulted in the development of a N dipping normal fault that is roughly aligned with

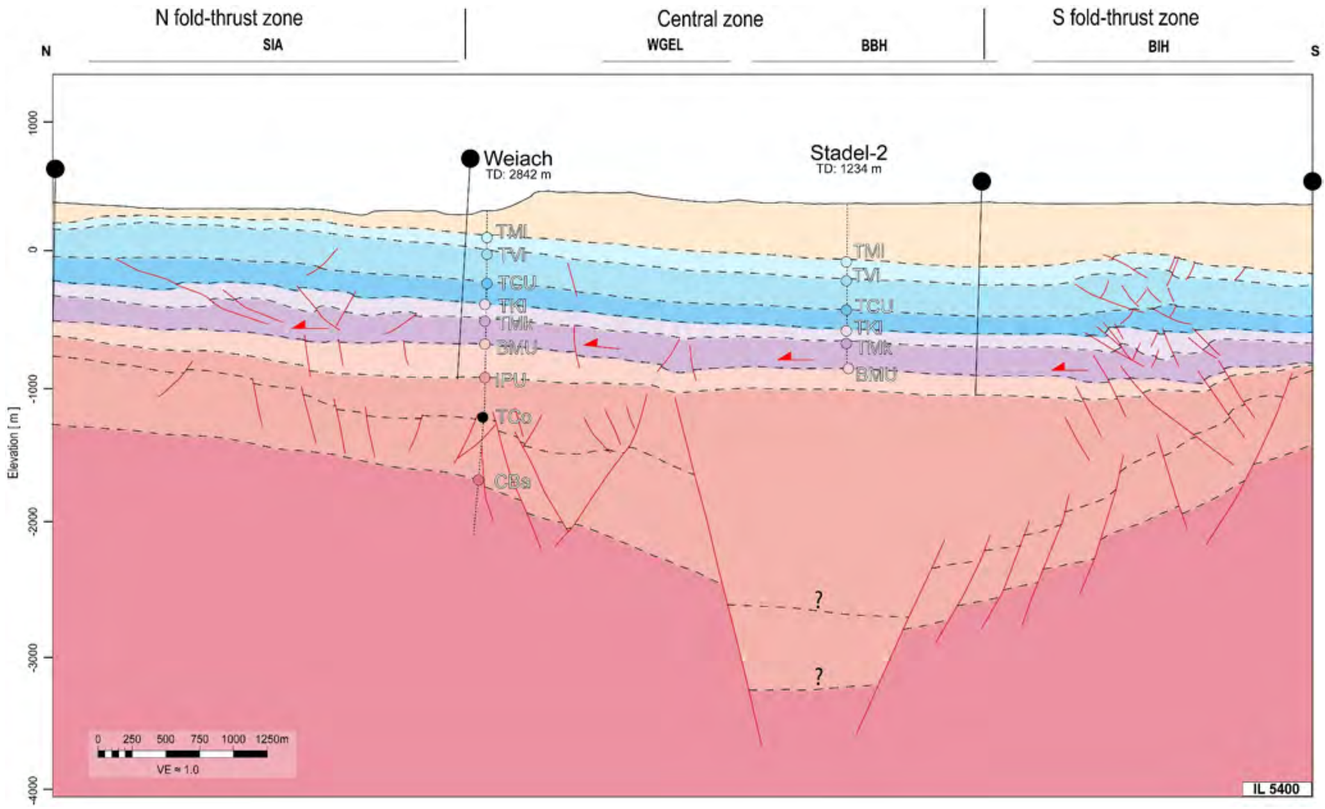

Figure 11. Balanced cross-section along depth-converted inline 5400 (located in Figure 6a). Pin lines define the three sectors for which shortening calculations were carried out (Table 1). SIA = Siglistorf Anticline; WGEL = Weiach-Glattfelden-Eglisau Lineament; BBH = Bach-Bulach Homocline; BIH = Baden-Irchel-Herdern triangle zone; TMl = Top Malm; Tvi = Top Villingen; TCU = Top Clay Unit (168.2_Baj_400); TKl = Top Klettgau; TMk = Top Muschelkalk; BMU = Base Mesozoic Unconformity; IPU = Intra-Permian Unconformity; Tco = Top Coal series; Cba = Top Crystalline Basement.

the BIH (Figure 3) but did not produce any localization of contractional deformation in such an eastern area (Malz et al., 2016).

5.2. N Fold-Thrust Zone

The overall geometry of the N fold-thrust zone is reminiscent of that obtained by analogue modeling of detachment-dominated thrusting interacting with basement steps (Figure 1e). Modeling evidence and field examples from the Jura fold and thrust belt suggest that the detachment can overcome this type of basement steps (both "upward" and "downward" with respect to thrust transport direction), to further propagate within the sedimentary cover of the adjacent block of the inherited basement fault (Caër et al., 2018; Schori et al., 2021). Therefore, although the N fold-thrust zone is located above a step produced by a S dipping fault in the underlying Permian-Carboniferous graben, seismic interpretation coupled with regional knowledge (Guellec et al., 1990) and published modeling results (Schori et al., 2021) suggest that the integrity of the detachment may have been preserved along the entire along-strike extension of this structure. The geometry of the composite pop-up forming the N fold-thrust zone is consistent with a décollement that allowed the Mesozoic rock panel, decoupled from the underlying upper Paleozoic sediments, to be shortened at this specific location where the detachment interacted with a substratum step but was not locked. The fact that structures closely resembling those of the N fold-thrust zone are produced by sandbox analogue modeling also suggests that composite pop-ups of that type could develop even independently of viscosity contrasts within the multilayer (which however are well known to occur in our natural example).

Table 1
Summary of Geological Section Balancing and Restoration, Including Deformed and Restored Lengths, Areas, and Shortening Values for the Mesozoic Succession Overlying the Muschelkalk Evaporites

Method	Area [m^2]	L0 [m]	Lf [m]	S [m]	S [%]
Area balancing	7779512	10071	9482	589	5.9
Line-length balancing		9667	9482	185	2.0

Note. The shortening obtained by line-length balancing represents the mean value calculated based on the following marker horizons: TMl = Top Malm; TVi = Top Villingen; TCU = Top Clay Unit (168.2_Baj_400); TKl = Top Klettgau; TMk = Top Muschelkalk. Pin lines shown in Figure 11 were used for the analysis. Lf = final length; L0 = restored length, S = Shortening.

Table 2
Detailed Results of the Geological Section Balancing by Areas and Horizons

		Line-length balancing				Area balancing		
Zone	Horizon	Lf [m]	L0 [m]	S [m]	S [%]	Area [m^2]	S [m]	S [%]
N fold-thrust zone (SIA)	TMl	3099	3113	14	0.5	227335	280	8.3
	Tvi	3099	3115	16	0.5	784104	280	8.3
	TCU	3099	3112	13	0.4	578418	280	8.3
	TKl	3099	3171	72	2.3	408880	280	8.3
	TMk	3099	3204	105	3.3	451778	280	8.3
	BMU	3099	3105	6	0.2	/	/	/
	IPU	3099	3102	3	0.1			
	Total	3099	3172	73	2.3	2450515	280	8.3
Central zone (WGEL and BBH)	TMl	3878	3885	8	0.2	516017	91	2.3
	Tvi	3878	3892	14	0.3	943292	91	2.3
	TCU	3878	3896	18	0.5	565297	91	2.3
	TKl	3878	3896	18	0.5	418017	91	2.3
	TMk	3878	3900	22	0.6	836913	91	2.3
	BMU	3878	3918	40	1.0	/	/	/
	IPU	3878	3901	23	0.6			
	Total	3878	3900	22	0.6	3279535	91	2.3
S fold-thrust zone (BIH)	TMl	2505	2549	44	1.7	303374	218	8.0
	Tvi	2505	2580	75	2.9	592357	218	8.0
	TCU	2505	2550	45	1.8	360805	218	8.0
	TKl	2505	2599	94	3.6	274911	218	8.0
	TMk	2505	2644	139	5.3	506009	218	8.0
	BMU	2505	2591	86	3.3	/	/	/
	IPU	2505	2619	114	4.3			
	Total	2505	2595	90	3.5	2037455	218	8.0

Note. Pin lines shown in Figure 11 were used for the analysis. Lf = final length; L0 = restored length, S = Shortening; TMl = Top Malm; TVi = Top Villingen; TCU = Top Clay Unit (168.2_Baj_400); TKl = Top Klettgau; TMk = Top Muschelkalk; BMU = Base Mesozoic Unconformity; IPU = Intra-Permian Unconformity.

The wide belt of thrusts and backthrusts forming the N fold-thrust zone is not compatible with a deeply rooted structure involving reverse fault slip passed directly from one or more reactivated, upper Paleozoic fault(s) to thrusts located in the Mesozoic sedimentary cover (e.g., McClay, 1995). At variance with the interpretation by Schöpfer et al. (2024), no major structures are seismically imaged in the Permian-Carboniferous units that could account for direct linkage of the N fold-thrust zone with shortening involving the underlying upper Paleozoic basin fill. The gently S dipping Base Mesozoic Unconformity underlying thrust-related folds affecting the Mesozoic strata clearly defines a shallow detachment controlled by the Triassic evaporites (Figures 8 and 11). Therefore, detachment-dominated thrusting occurred within the study area, despite the limited thickness (well below the critical value of 150 m suggested by Sommaruga et al., 2017) of the Triassic salt and of the entire Muschelkalk evaporite interval.

5.3. S Fold-Thrust Zone

The S fold-thrust zone is located above a major N dipping normal fault of the CFT and consists of vertically superposed fish-tail structures involving the Middle Triassic-Jurassic series. The geometry of the oppositely dipping, low-displacement reverse faults resembles that of structures occurring in deforming multilayers characterized by substantial competence (i.e., viscosity) contrasts. Modeling work summarized by Price and Cosgrove (1990) demonstrates the coexistence of folding and faulting during the same deformation, a wide range of fold-thrust relative timing relationships being possible. The occurrence of buckling (Biot, 1961; Ramberg, 1960,

1964) well explains disharmonic folding of the two competent panels above and below the Clay Unit (Figure 9). Various studies pointed out the fundamental role played by mechanically dominant members in buckle folding (e.g., Butler et al., 2020; Mazzoli et al., 2001; Morley, 1994), fold wavelengths being typically controlled by the thickness of such more competent "control units" (Cobbold, 1975; Price & Cosgrove, 1990). In the case of the Mesozoic multilayer involved in the S fold-thrust zone, the incompetent lithology of the Clay Unit allowed significant decoupling of the deformation between a lower "control unit" (thick-bedded to massive limestones and dolostones of the Upper Muschelkalk) and an upper "control unit" consisting of thick-bedded to massive limestones of the Villigen Fm and Upper Malm. The Clay Unit appears to have been shortened and locally thickened by ductile strain between the two disharmonically folded, competent rock panels located above and below it. The upper competent panel is antiformally folded, while the lower competent panel is synformally folded, resulting in a tectonically thickened Clay Unit in the core of both folds (Figure 9). This deformation is schematically represented by an ellipse in Figure 9a as if it was roughly pure shear, although the actual distribution of finite strain within incompetent units involved in buckling is well known to be more complex (Ramsay & Huber, 1987; in this specific case, the complexity is further increased by the strain gradient that must occur into and out of the tectonically thickened zone). It may be envisaged that the thickness of the incompetent Clay Unit was sufficient to allow disharmonic folding of the two competent rock panels located above and below it—that is, the zones of contact strain (Ramsay & Huber, 1987) of the two competent beams surrounding the Clay Unit did not overlap. The thickness of the Muschelkalk appears to be substantially reduced below the syncline (Figure 9b). This thickness variation is interpreted as due to the mobility of the evaporite component of the Muschelkalk, which includes several tens of meters of halite (encountered in all the four boreholes of Figure 4 which are located within 2.5 km from the S fold-thrust zone). Salt weld development (i.e., salt thickness reduced to near zero) at this position may be interpreted as resulting from salt withdrawal produced by "downfolding" of the lower competent panel underlying the Clay Unit, and/or salt flow in the footwall of reverse faults because of hanging wall loading. In any case, taking into account the significant along-strike continuity of the zone of reduced salt thickness, salt welding would add an additional constraint on deformation by changing (increasing) the friction along the portion of the basal décollement where the salt thickness has been significantly or completely reduced. Higher friction, in turn, leads to build up of structural relief associated with stress concentration.

Reverse faults offsetting the upper Paleozoic basin fill at the S fold-thrust zone document mild shortening of the CFT. However, seismic interpretation within the Permian-Carboniferous succession provided no evidence of reactivation of inherited normal faults and upward thrust propagation from their pre-existing tip lines (Figure 9). Numerous reverse faults interpreted within the Permian-Carboniferous succession also offset the Base Mesozoic Unconformity. These faults may be envisaged as resulting from buttressing against major, CFT steep normal faults that appear to remain essentially locked (Figures 6 and 9). Although restoring the offset Base Mesozoic Unconformity also restores the substratum to an unfaulted state, considering seismic resolution in the Permian-Carboniferous succession implies that some of the observed reverse faults could also have originated as small-offset, antithetic normal faults.

5.4. Modes and Relative Chronology of Neogene Shortening

Late-stage, thick-skinned and ramp-dominated reverse/oblique-slip faulting within the study area was accompanied by gentle folding of the coupled Permian-Carboniferous basin fill and overlying Mesozoic strata, and gentle tilting of rock panels associated with fault-related deformation (as it is observed along the WGEL; compare Figures 11 and 12a). Most high-angle faults picked on seismic data do not offset the Clay Unit. This feature is interpreted in terms of rheological behavior of this unit, which in most cases appears to accommodate the strain without evident fault displacement at the seismic scale (see also Roche et al., 2020). However, few larger faults also offset the Clay Unit (as shown by displaced base and/or Top Clay Unit), whose internal reflectors are dominated by multiples and therefore cannot be used in structural interpretation.

Concerning fold-thrust structures, substantial thickness changes are associated with blind thrusting and multilayer folding characterized by marked competence contrasts (Figure 11). In this instance, area balancing provides more meaningful results than line-length balancing of individual stratigraphic markers. Comparing line-length and area balancing results (Tables 1 and 2) indicates that a significant amount of the total shortening is accommodated by internal strain of the rocks. This is consistent with the observed core-scale deformation of rocks sampled with the boreholes, which is characterized by a variable (depending on formation) but generally widespread occurrence of small faults, micro-faults, and tectonic foliation, with a large predominance of shear planes displaying reverse-

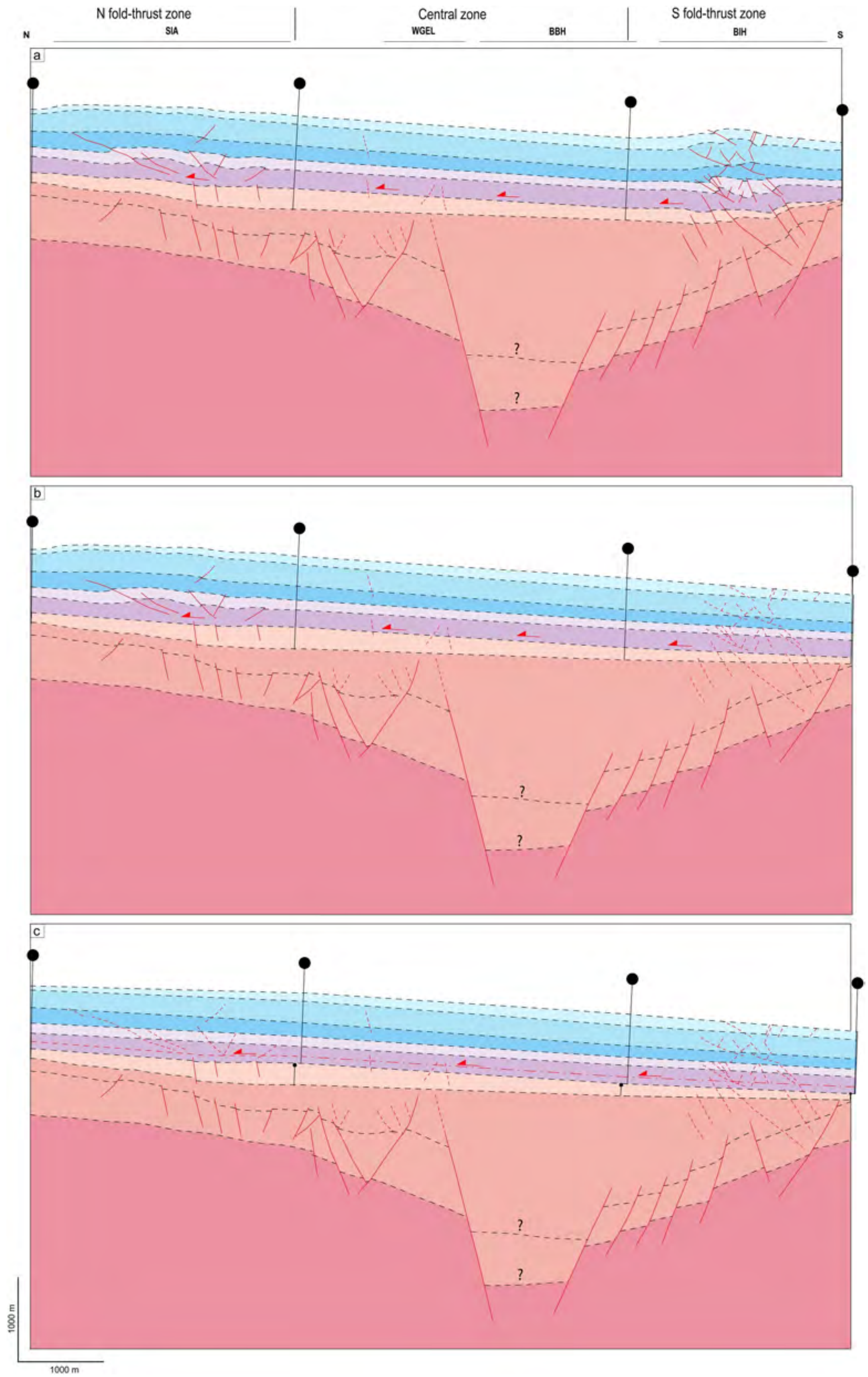
N fold-thrust zone
SIA
Central zone
WGEL
BBH
S fold-thrust zone
BIH
N
S
a
?
?
b
?
?
c
?
?
1000 m
1000 m

Figure 12.

fault kinematics (Decker et al., 2022). Such a core-scale deformation is recorded in boreholes located away from the main fold-thrust zones, including in the macroscopically "undeformed" Mesozoic rock panel forming the Bachs-Bülach Homocline. This latter is underlain by a thrust detachment and therefore not surprisingly affected by distributed horizontal shortening-related strain. A further layer-parallel shortening contribution could be associated with late-stage, thick-skinned shortening, as indicated by core-scale deformation features affecting also Lower Triassic and Permian stratigraphic units underlying the Muschelkalk evaporite décollement (Decker et al., 2022). The implications are that: (a) the original (i.e., pre-deformational) thickness of the formations cannot be precisely defined, and those used in area balancing and restoration represent maximum values; (b) the shortening values obtained by area balancing must be considered as minimum estimates (as already mentioned in Section 3.4); (c) the areas of marked seismic scale deformation and tectonic thickening (not penetrated by wells) should be characterized by a greater density of meso- and micro-scale structures, resulting in a cumulative higher internal strain; and (d) localized deformation at the mesoscopic and microscopic scales resulted in substantial distributed strain at the regional scale (always considering we are dealing with a rather modest total shortening of around 6%; therefore the terms "substantial" and "significant" must be considered in a relative way here). On the other hand, line-length balancing of individual horizons is important for evaluating the degree of substratum-cover coupling (i.e., by comparing shortening of the Intra-Permian and Base Mesozoic unconformities with that of the Mesozoic multilayer overlying the Muschelkalk evaporites). For the N fold-thrust zone, the shortening measured by line-length balancing at Top Muschelkalk level is substantially larger than that measured along the Base Mesozoic Unconformity and the Intra-Permian Unconformity (Table 2), thus implying detachment-dominated thrusting of the Mesozoic succession overlying the Triassic evaporites (although very gentle folding of the Base Mesozoic Unconformity at this location may be associated with late-stage mild shortening of the whole CFT and was therefore restored in Figure 12b). On the contrary, for the S fold-thrust zone, the shortening measured by line-length balancing at Top Muschelkalk level is generally consistent with that measured along the Base Mesozoic Unconformity and the Intra-Permian Unconformity (Table 2). This indicates that shortening of the Mesozoic succession is rooted into the underlying upper Paleozoic basin fill. Several reverse faults offsetting the Base Mesozoic Unconformity terminate (i.e., have their upper tip) within the Muschelkalk evaporite décollement level, which appears to have favored a soft linkage among fault segments located below and above it. This is a fundamental feature, as planar faults passing from the Paleozoic succession straight into the Jurassic one would not produce the narrow belt of folds and fishtail structures forming the BIH triangle zone. The observed structural pattern suggests instead that the décollement was still active during the early stages of deep-seated shortening, and that its interaction with the reverse fault splays propagating upward from the Paleozoic succession localized deformation in the overlying Mesozoic multilayer. It is worth noting that substantial thrust displacement could not have been transferred northward from the S fold-thrust zone to the Muschelkalk evaporite décollement because: (a) the shortening produced by the reverse faults offsetting the Base Mesozoic Unconformity is rather modest and, as already mentioned above, roughly balances that of the overlying Mesozoic horizons involved in the BIH triangle zone (Table 2), and (b) there is no seismic evidence of contractional reactivation of the normal fault underlying the S fold-thrust zone (which anyway is N dipping, and therefore unlikely to be able to transfer any reverse slip component to the décollement level located north of it; Figure 9). In essence, there is no excess shortening to be passed to the décollement and to produce detachment-related, thin-skinned structures to the north. On the other hand, although most reverse fault segments affecting the overlying Mesozoic series are not directly connected (i.e., hard linked) with those offsetting the Base Mesozoic Unconformity, a few major faults did propagate through the Muschelkalk evaporite décollement. This was locally

Figure 12. Sequential restoration of the balanced cross-section of Figure 11, summarizing main deformation stages that led to the development of the N and S fold-thrust zones, and post-thrusting fault splays at the WGEL site (strata overlying Top Malm marker are not shown). (a) Restoration showing the tectonic setting predating the development of the fault splays offsetting the Mesozoic succession at the WGEL site. Bulk crustal shortening, reverse faulting within the upper Paleozoic basin fill and development of the S fold-thrust zone (at a site of strong interaction of the décollement with substratum features) may have occurred between ∼8 and ∼4 Ma, following the termination of detachment-dominated thrusting within the study area (at ∼8 Ma according to Madritsch et al., 2024). (b) Restoration showing the tectonic setting at ∼8 Ma. Detachment-dominated thrusting and development of the N fold-thrust zone at a site of weak interaction of the décollement with substratum features, shown in this diagram, may have occurred between ∼12 and ∼8 Ma (Madritsch et al., 2024). (c) Restoration at Middle Miocene times (∼15 Ma), showing the pre-orogenic setting (i.e., postdating the regional flexure associated with foreland basin development, and predating the onset of thrusting and folding). SIA = Siglistorf Anticline; WGEL = Weiach-Glattfelden-Eglisau Lineament; BBH = Bach-Bulach Homocline; BIH = Baden-Irchel-Herdern triangle zone; TMl = Top Malm; TVi = Top Villingen; TCU = Top Clay Unit (168.2_Baj_400); TKl = Top Klettgau; TMk = Top Muschelkalk; BMU = Base Mesozoic Unconformity; IPU = Intra-Permian Unconformity; TCo = Top Coal series; CBa = Top Crystalline Basement.

juxtaposed to other terms of the stratigraphic succession (Figure 9), most probably compromising the quality of the detachment.

The reconstructed kinematic evolution based on seismic interpretation implies the "rooted" S fold-thrust zone to have formed later than the "detached" N fold-thrust zone (Figure 12). This is consistent with the backstepping thrust sequence suggested—although based on different considerations—by Malz et al. (2015). Numerical modeling work by Caër et al. (2018) investigated the stress concentration arising at substratum steps and the frictional conditions needed for different scenarios. A major outcome of such a work is that topographic relief and friction along the faults are the main drivers promoting or inhibiting the build-up of structural relief and forward propagation of the basal décollement. According to their modeling results, imbrication and building of structural relief at a site of a "downward" basement step may have resulted in the formation of the faulted Lägern Anticline in the hanging wall of the Jura Main Thrust (south of our study area; Figure 3b). The development of multiple thrust ramps at that location would have eventually created the critical topography necessary to further propagate the basal décollement, leading to the formation of the N fold-thrust zone at the next—"upward" in this instance—substratum step located to the NNW (within our study area; Siglistorf Anticline in Figure 3). Based on seismic interpretation and consistent with this reconstruction, no major substratum step was present at the (future) site of the S fold-thrust zone (Baden-Irchel-Herdern triangle zone in Figure 3) during detachment-dominated thrusting (Figure 12b). Concentration of the deformation at the S fold-thrust zone occurred only later, when deep-seated deformation affecting the upper Paleozoic basin fill led to the development of reverse fault splays offsetting the Base Mesozoic Unconformity (Figure 12a). Within this framework, the development of the S fold-thrust zone does not merely represent a case of backstepping thrust propagation. Rather, it marks the switch from detachment-dominated thrusting of the Mesozoic sedimentary cover to deep-seated shortening involving the sub-décollement Permian-Carboniferous trough in the study area. In both the N and S fold-thrust zones, complex lateral propagation of structural features from sites of more effective interaction of the décollement with substratum steps/faults resulted in highly segmented, non-cylindrical assemblages (Figure 5b). The extraordinary quality of the 3D seismic data used in this study allows documenting in detail the structures produced in the different cases of: (a) weak interaction at extensional fault steps, and (b) strong interaction with late-stage reverse faults, eventually leading to locking of the evaporite décollement. As such, this work provides new insights into the modes of deactivation and inhibition of thrust detachments during the switch to thick-skinned deformation. At a regional scale, this switch implies a major change in the modes of deformation, from basement underthrusting—and underplating beneath the External Basement Massifs of the Alps—to bulk crustal shortening affecting the entire Jura Mts.-Swiss Molasse Basin system (Mosar, 1999).

6. Conclusions

Different degrees of interaction between the Middle Triassic evaporite décollement level and sub- décollement, inherited/newly formed faults produced a marked contrast in structural style between the N fold-thrust zone (broad, composite pop-up structure developed by detachment-dominated thrusting) and the S fold-thrust zone (fishtail structures organized in a subvertical, narrow belt). The substratum structure underlying the N fold-thrust zone consists of a set of "upward" (with respect to thrust transport direction) substratum steps associated with a S dipping normal fault system. This set of steps controlled thrust ramp and backthrust nucleation, however without locking the detachment. Therefore, this type of substratum-cover interaction may be described as "weak interaction." Since the substratum structure underlying the S fold-thrust zone was not extensionally reactivated and did not form a step at the time of thin-skinned thrusting within the studied volume, the detachment could propagate from the Jura Main Thrust (located south of our study area) to the N fold-thrust zone. Therefore, the detachment-related N fold-thrust zone formed first within the studied rock volume. Later crustal shortening produced the propagation of reverse faults from the upper Paleozoic succession into the Mesozoic strata. Deformation of the Permian-Carboniferous basin fill occurred substantially around the southern edge faults of the Constance-Frick Trough. This became a site of substratum-cover "strong interaction," giving rise to the S fold-thrust zone. Our results suggest that the shallow décollement active during thin-skinned thrusting was not just abandoned as deformation migrated to deeper crustal levels. Rather, such a décollement probably played a major role during incipient deep-seated shortening. Its interaction with faults propagating from sub-décollement levels focused layer-parallel shortening (accommodated by coeval buckle folding and reverse faulting) within the Mesozoic sedimentary cover at the S fold-thrust zone. Syn-kinematic salt mobility may have contributed to additional concentration of strain along a narrow belt of Mesozoic strata by increasing the friction along the underlying portion of the décollement with reduced evaporite thickness. Eventually, hard linkage/propagation of a few fault segments cutting across the Base Mesozoic Unconformity up to the Jurassic terms of the succession produced the local juxtaposition of the Middle Triassic evaporites with different formations. Further pinning of the detachment was produced by reverse/oblique-slip fault segments that nucleated in the proximity of pre-existing Paleozoic faults and cut across the Middle Triassic décollement level, as it occurred along the Weiach-Glattfelden-Eglisau Lineament.

The weak versus strong substratum-cover interaction documented in this study represents a detailed record of the transition from detachment-dominated thrusting of the sedimentary cover to deeply rooted deformation associated with bulk crustal shortening. The unraveled modes of substratum-cover interaction provide new insights into deformation style variability in fold and thrust belts, beyond the contingent thin- versus thick-skinned thrusting debate.

Data Availability Statement

Seismic data used for interpretation in the study are available at Zambrano et al. (2024). Supporting data for Zambrano et al. (2024)—Tectonics—Modes of deformation in sedimentary multilayers interacting with sub-décollement structures: insights from 3D seismic interpretation in the eastern Jura fold and thrust belt: Seismic lines from the Nördlich Lärgern seismic volume [Dataset]. Figshare. https://doi.org/10.6084/m9.figshare.26021614.

Acknowledgments
Useful comments and suggestions by Tectonics editor Djordje Grujic, associate editor Olivier Lacombe and reviewers Jonas Kley, Nicolas Espurt and Katerina Schöpfer allowed us to substantially improve the paper. We acknowledge Nagra for providing the data used in this study and for the permission to share our results. The use of Move software granted by Petroleum Experts is also acknowledged. Open access publishing facilitated by Universita degli Studi di Camerino, as part of the Wiley - CRUI-CARE agreement.

References

Adams, A., & Diamond, L. W. (2019). Facies and depositional environments of the Upper Muschelkalk (Schinznach Formation, Middle Triassic) in northern Switzerland. *Swiss Journal of Geosciences*, *112*(2–3), 357–381. https://doi.org/10.1007/s00015-019-00340-7

Allenbach, R. P. (2001). Syn-sedimentary tectonics in an epicontinental sea: A new interpretation of the Oxfordian basins of northern Switzerland. In *Eclogae Geologicae Helvetiae* (Vol. 94, pp. 265–287).

Allenbach, R. P. (2002). The ups and downs of "Tectonic Quiescence"—Recognizing differential subsidence in the epicontinental sea of the Oxfordian in the Swiss Jura Mountains. *Sedimentary Geology*, *150*(3–4), 323–342. https://doi.org/10.1016/S0037-0738(01)00202-0

Balansa, J., Espurt, N., Hippolyte, J.-C., Philip, J., & Caritg, S. (2022). Structural evolution of the superimposed Provençal and Subalpine fold-thrust belts (SE France). *Earth-Science Reviews*, *227*, 103972. https://doi.org/10.1016/j.earscirev.2022.103972

Barnes, P. M., & Nicol, A. (2004). Formation of an active thrust triangle zone associated with structural inversion in a subduction setting, eastern New Zealand. *Tectonics*, *23*(1), TC1015. https://doi.org/10.1029/2002TC001449

Becker, A. (2000). The Jura Mountains—An active foreland fold-and-thrust belt? *Tectonophysics*, *321*(4), 381–406. https://doi.org/10.1016/s0040-1951(00)00089-5

Biot, M. A. (1961). Theory of folding of stratified viscoelastic media and its implications in tectonics and orogenesis. *Geological Society of America Bulletin*, *72*(11), 1595–1620. https://doi.org/10.1130/0016-7606(1961)72[1595:tofosv]2.0.co;2

Butler, R. W. (1982). The terminology of structures in thrust belts. *Journal of Structural Geology*, *4*(3), 239–245. https://doi.org/10.1016/0191-8141(82)90011-6

Butler, R. W. H. (1989). The influence of preexisting basin structure on thrust system evolution in the Western Alps. In M. A. Cooper & G. D. Williams (Eds.), *Geological Society, London, Special Publications*. Geological Society of London Special Publication (Vol. 44, pp. 105–122). https://doi.org/10.1144/gsl.sp.1989.044.01.07

Butler, R. W. H., Bond, C. E., Cooper, M. A., & Watkins, H. (2020). Fold–thrust structures–where have all the buckles gone? *Geological Society, London, Special Publications*, *487*(1), 21–44. https://doi.org/10.1144/sp487.7

Butler, R. W. H., & Paton, D. A. (2010). Evaluating lateral compaction in deepwater fold and thrust belts: How much are we missing from "nature's sandbox". *Geological Society of America Today*, *20*, 4–9. https://doi.org/10.1130/GSATG77A.1

Buxtorf, A. (1916). Prognosen und Befunde beim Hauensteinbasis-und Grenchenbergtunnel und die Bedeu-tung der letzteren für die Geologie des Juragebirges. *Verhandlungen der Naturforschenden Gesellschaft in Basel*, *27*, 184–205.

Caër, T., Souloumiac, P., Maillot, B., Leturmy, P., & Nussbaum, C. (2018). Propagation of a fold-and-thrust belt over a basement graben. *Journal of Structural Geology*, *115*, 121–131. https://doi.org/10.1016/j.jsg.2018.07.007

Cobbold, P. R. (1975). Fold propagation in single embedded layers. *Tectonophysics*, *27*(4), 333–351. https://doi.org/10.1016/0040-1951(75)90003-7

Costa, E., & Vendeville, B. C. (2002). Experimental insights on the geometry and kinematics of fold-and-thrust belts above weak, viscous evaporitic decollement. *Journal of Structural Geology*, *24*(11), 1729–1739. https://doi.org/10.1016/s0191-8141(01)00169-9

Coward, M. P., De Donatis, M., Mazzoli, S., Paltrinieri, W., & Wezel, F. C. (1999). Frontal part of the northern Apennines fold and thrust belt in the Romagna-Marche area (Italy): Shallow and deep structural styles. *Tectonics*, *18*(3), 559–574. https://doi.org/10.1029/1999tc900003

Davis, D., Suppe, J., & Dahlen, F. A. (1983). Mechanics of fold-and-thrust belts and accretionary wedges. *Journal of Geophysical Research*, *88*(B2), 1153–1172. https://doi.org/10.1029/jb088ib02p01153

Decker, K., Schneeberger, R., & Madritsch, H. (2022). Paleo-strain reconstruction from drill core mapping and their relevance for northern Switzerland. In *Abstract Volume, 55. 20th Swiss Geoscience Meeting, 18–20 November 2022, Lausanne. For Northern Switzerland*.

Egan, S. S., Kane, S., Budding, T. S., Williams, G. D., & Hodgetts, D. (1999). Computer modelling and visualisation of the structural deformation caused by movement along geological faults. *Computers & Geosciences*, *25*(3), 283–297. https://doi.org/10.1016/S0098-3004(98)00125-3

Egli, D., Mosar, J., Ibele, T., & Madritsch, H. (2016). The role of precursory structures on Tertiary deformation in the Black Forest-Hegau region. *International Journal of Earth Sciences*, *106*(7), 2297–2318. https://doi.org/10.1007/s00531-016-1427-8

Eichkitz, C. G., Schneider, S., Hölker, A. B., Birkhäuser, P., & Madritsch, H. (2020). On the impact of alternative seismic time imaging methods on subsurface fault mapping in the northernmost Molasse Basin, Switzerland. *Interpretation*, *8*(4), SQ1–SQ13. https://doi.org/10.1190/int-2019-0305.1

Erslev, E. A. (1991). Trishear fault-propagation folding. *Geology*, *19*(6), 617–620. https://doi.org/10.1130/0091-7613(1991)019<0617:TFPF>2.3.CO;2

Fabbi, S., & Smeraglia, L. (2019). Pop-up structure in massive carbonate-hosted fold-and-thrust belt: Insight from field mapping and 2D kinematic model in the central Apennines. *Journal of Structural Geology*, *126*, 258–271. https://doi.org/10.1016/j.jsg.2019.06.011

Giamboni, M., Ustaszewski, K., Schmid, S. M., Schumacher, M. E., & Wetzel, A. (2004). Plio-Pleistocene transpressional reactivation of Paleozoic and Paleogene structures in the Rhine-Bresse transform zone (northern Switzerland and eastern France). *International Journal of Earth Sciences*, *93*(2), 207–223. https://doi.org/10.1007/s00531-003-0375-2

Graveleau, F., Malavieille, J., & Dominguez, S. (2012). Experimental modelling of orogenic wedges: A review. *Tectonophysics*, *538*, 1–66. https://doi.org/10.1016/j.tecto.2012.01.027

Groshong, R. H., Withjack, M. O., Schlische, R. W., & Hidayah, T. N. (2012). Bed length does not remain constant during deformation: Recognition and why it matters. *Journal of Structural Geology*, *41*, 86–97. https://doi.org/10.1016/j.jsg.2012.02.009

Guellec, S., Lajat, D., Mascle, A., Roure, F., & Tardy, M. (1990). Deep seismic profiling and petroleum potential in the western Alps: Constraints with ECORS data, balanced cross-sections and hydrocarbon modeling. In *The potential of deep seismic profiling for hydrocarbon exploration* (pp. 425–437).

Jamison, W. R. (1993). Mechanical stability of the triangle zone: The backthrust wedge. *Journal of Geophysical Research*, *98*(B11), 20015–20030. https://doi.org/10.1029/93JB01233

Jaquet, Y., Bauville, A., & Schmalholz, S. M. (2014). Viscous overthrusting versus folding: 2-D quantitative modeling and its application to the Helvetic and Jura fold and thrust belts. *Journal of Structural Geology*, *62*, 25–37. https://doi.org/10.1016/j.jsg.2014.01.010

Jordan, P. (1992). Evidence for large-scale decoupling in the Triassic evaporites of Northern Switzerland: An overview. *Eclogae Geologicae Helvetiae*, *85*(3), 677–693.

Jordan, P., & Deplazes, G. (2019). Lithostratigraphy of consolidated rocks expected in the Jura Ost, Nördlich Lägern and Zürich Nordost Regions. In *Nagra Arbeitsbericht NAB 19–14*.

Jordan, P., Malz, A., Heuberger, S., Pietsch, J., Kley, J., & Madritsch, H. (2015). Arbeitsbericht nab 14-105. Regionale geologische Profilschnitte durch die Nordschweiz und 2d-Bilanzierung der Fernschubdeformation im östlichen Faltenjura: Arbeitsbericht zu sgt-etappe 2. In *Arbeitsbericht NAB 14-105*. Nagra.

Lacombe, O., & Bellhasen, N. (2016). Thick-skinned tectonics and basement-involved fold–thrust belts: Insights from selected Cenozoic orogens. *Geological Magazine*, *153*(5–6), 763–810. https://doi.org/10.1017/S0016756816000078

Lacombe, O., & Mouthereau, F. (2002). Basement-involved shortening and deep detachment tectonics in forelands of orogens: Insights from recent collision belts (Taiwan, western Alps, Pyrenees). *Tectonics*, *21*(4), 1030. https://doi.org/10.1029/2001TC901018

Laubscher, H. P. (1986). The eastern Jura: Relations between thin-skinned and basement tectonics, local and regional. *Geologissche Rundschau*, *75*(3), 535–553. https://doi.org/10.1007/bf01820630

Looser, N., Madritsch, H., Guillong, M., Laurent, O., Wohlwend, S., & Bernasconi, S. M. (2021). Absolute age and temperature constraints on deformation along the basal décollement of the Jura fold-and- thrust belt from carbonate U-Pb dating and clumped isotopes. *Tectonics*, *40*(3), e2020TC006439. https://doi.org/10.1029/2020tc006439

Madritsch, H. (2015). Outcrop-scale fracture systems in the Alpine foreland of central northern Switzerland: Kinematics and tectonic context. *Swiss Journal of Geosciences*, *108*(2–3), 155–181. https://doi.org/10.1007/s00015-015-0203-2

Madritsch, H., Looser, N., Schneeberger, R., Wohlwend, S., Guillong, M., & Malz, A. (2024). Reconstructing the evolution of foreland fold-and-thrust belts using U-Pb calcite dating: An integrated case-study from the easternmost Jura Mountains (Switzerland). *Tectonics*, *43*(5). https://doi.org/10.1029/2023TC008181

Madritsch, H., Naef, H., Meier, B., Franzke, H. J., & Schreurs, G. (2018). Architecture and kinematics of the Constance-Frick Trough (northern Switzerland): Implications for the formation of post-Variscan basins in the foreland of the Alps and scenarios of their Neogene reactivation. *Tectonics*, *37*(7), 2197–2220. https://doi.org/10.1029/2017tc004945

Madritsch, H., Schmid, S. M., & Fabbri, O. (2008). Interactions between thin- and thick-skinned tectonics at the northwestern front of the Jura fold-and-thrust belt (eastern France). *Tectonics*, *27*(5), TC5005. https://doi.org/10.1029/2008tc002282

Malz, A., Madritsch, H., & Kley, J. (2015). Improving 2D seismic interpretation in challenging settings by integration of restoration techniques: A case study from the Jura fold-and-thrust belt (Switzerland). *Interpretation*, *3*(4), SAA37–SAA58. https://doi.org/10.1190/int-2015-0012.1

Malz, A., Madritsch, H., Meier, B., & Kley, J. (2016). An unusual triangle zone in the external northern Alpine foreland (Switzerland): Structural inheritance, kinematics and implications for the development of the adjacent Jura fold-and-thrust belt. *Tectonophysics*, *670*, 127–143. https://doi.org/10.1016/j.tecto.2015.12.025

Mazzoli, S., Barkham, S., Cello, G., Gambini, R., Mattioni, L., Shiner, P., & Tondi, E. (2001). Reconstruction of continental margin architecture deformed by the contraction of the Lagonegro Basin, southern Apennines, Italy. *Journal of the Geological Society*, *158*(2), 309–319. https://doi.org/10.1144/jgs.158.2.309

McClay, K. R. (1992). Glossary of thrust tectonics terms. In K. R. McClay (Ed.), *Thrust tectonics*. Chapman & Hall.

McClay, K. R. (1995). The geometries and kinematics of inverted fault systems: A review of analogue model studies. *Geological Society, London, Special Publications*, *88*(1), 97–118. https://doi.org/10.1144/GSL.SP.1995.088.01.07

Meyer, B., Lacassin, R., Brulhet, J., & Mouroux, B. (1994). The Basel 1356 earthquake: Which fault produced it? *Terra Nova*, *6*(1), 54–63. https://doi.org/10.1111/j.1365-3121.1994.tb00633.x

Morley, C. K. (1994). Fold-generated imbricates: Examples from the Caledonides of Southern Norway. *Journal of Structural Geology*, *16*(5), 619–631. https://doi.org/10.1016/0191-8141(94)90114-7

Mosar, J. (1999). Present-day and future tectonic underplating in the western Swiss Alps: Reconciliation of basement/wrench-faulting and décollement folding of the Jura and Molasse Basin in the Alpine foreland. *Earth and Planetary Science Letters*, *173*(3), 143–155. https://doi.org/10.1016/s0012-821x(99)00238-1

Nagra. (2014). SGT-Etappe 2: Vorschlag weiter zu untersuchender geologischer Standortgebiete mit zugehörigen Standortarealen für die Oberflächenanlage. In *Geologische Grundlagen—Dossier II: Sedimentologische und tektonische Verhältnisse*. Nagra Tech. Ber. NTB 14-02.

Nagra. (2019). Preliminary horizon and structure mapping of the Nagra 3D seismics NL-16 (Nördlich Lägern) in time domain. In *Nagra Arbeitsbericht NAB 18-35*.

Pfiffner, O. A., Erard, P. F., & Stauble, M. (1997). Two cross sections through the Swiss Molasse Basin. In O. A. Pfiffner, P. Lehner, P. Heitzmann, S. Mueller, & A. Steck (Eds.), *Deep Structure of the Swiss Alps: Results of NRP 20* (pp. 64–71). Birkhäuser Verlag.

Philippe, Y., Colletta, B., Deville, E., & Mascle, A. (1996). The Jura fold-and-thrust belt: A kinematic model based on map-balancing. In P. Ziegler & F. Horvath (Eds.), *Peri-Tethys Memoir 2—Structure and Prospects of Alpine Basins and Forelands* (pp. 235–261). Mémoires du Museum National d'Histoire Naturelle. no. 170.

Price, N. J., & Cosgrove, J. W. (1990). *Analysis of geological structures*. Cambridge University Press.

Ramberg, H. (1960). Relationships between length of arc and thickness of ptygmatically folded veins. *American Journal of Science*, *258*(1), 36–46. https://doi.org/10.2475/ajs.258.1.36

Ramberg, H. (1964). Selective buckling of composite layers with contrasted rheological properties, a theory for simultaneous formation of several orders of folds. *Tectonophysics*, *1*(4), 307–341. https://doi.org/10.1016/0040-1951(64)90020-4

Ramsay, J. G., & Huber, M. I (1987). *The techniques of modern structural geology: Folds and fractures* (Vol. 2). Academic Press.

Roche, V., Childs, C., Madritsch, H., & Camanni, G. (2020). Layering and structural inheritance controls on fault zone structure in three dimensions: A case study from the northern Molasse Basin, Switzerland. *Journal of the Geological Society*, *177*(3), 493–508. https://doi.org/10.1144/jgs2019-052

Rotstein, Y., & Schaming, M. (2004). Seismic reflection evidence for thick-skinned tectonics in the northern Jura. *Terra Nova*, *16*(5), 250–256. https://doi.org/10.1111/j.1365-3121.2004.00560.x

Schöpfer, K., Decker, K., Nazari, F., & Madritsch, H. (2024). 3D-seismic evidence for thick-skinned tectonics in a "classic" thin skinned tectonics region (external Alpine foreland, Switzerland). *Terra Nova*, *36*(3), 217–229. https://doi.org/10.1111/ter.12701

Schori, M., Zwaan, F., Schreurs, G., & Mosar, J. (2021). Pre-existing basement faults controlling deformation in the Jura Mountains fold-and-thrust belt: Insights from analogue models. *Tectonophysics*, *814*, 228980. https://doi.org/10.1016/j.tecto.2021.228980

Simm, R., & Bacon, M. (2014). *Seismic amplitude: An interpreter's handbook*. Cambridge University Press.

Sommaruga, A., Mosar, J., Schori, M., & Gruber, M. (2017). The role of the Triassic evaporites underneath the North Alpine Foreland. In *Permo-Triassic Salt Provinces of Europe, North Africa and the Atlantic Margins* (pp. 447–466). Elsevier.

Swisstopo. (2005). *Tektonische Karte der Schweiz 1: 500 000*. Federal Office of Topography Swisstopo.

Ustaszewski, K., & Schmid, S. M. (2006). Control of preexisting faults on geometry and kinematics in the northernmost part of the Jura fold-and-thrust belt. *Tectonics*, *25*(5), TC5003. https://doi.org/10.1029/2005TC001915

Ustaszewski, K., & Schmid, S. M. (2007). Latest Pliocene to recent thick-skinned tectonics at the Upper Rhine Graben—Jura Mountains junction. *Swiss Journal of Geosciences*, *100*(2), 293–312. https://doi.org/10.1007/s00015-007-1226-0

von Hagke, C., & Malz, A. (2018). Triangle zones–geometry, kinematics, mechanics, and the need for appreciation of uncertainties. *Earth-Science Reviews*, *177*, 24–42. https://doi.org/10.1016/j.earscirev.2017.11.003

Watkins, H., Butler, R. W., & Bond, C. E. (2017). Using laterally compatible cross sections to infer fault growth and linkage models in foreland thrust belts. *Journal of Structural Geology*, *96*, 102–117. https://doi.org/10.1016/j.jsg.2017.01.010

Wetzel, A., Allenbach, R., & Allia, V. (2003). Reactivated basement structures affecting the sedimentary facies in a tectonically "quiescent" epicontinental basin: An example from NW Switzerland. *Sedimentary Geology*, *157*(1–2), 153–172. https://doi.org/10.1016/s0037-0738(02)00230-0

Zambrano, M., Mazzoli, S., Mosar, J., & Pedini, M. (2024). Supporting data for Zambrano et al. 2024—Tectonics—Modes of deformation in sedimentary multilayers interacting with sub-décollement structures: Insights from 3D seismic interpretation in the eastern Jura fold and thrust belt: Seismic lines from the Nördlich Lärgern seismic volume [Dataset]. *Figshare*. https://doi.org/10.6084/m9.figshare.26021614

Zimmerli, G. N., Wohlwend, S., Deplazes, G., Wetzel, A., Francescangeli, F., & Foubert, A. (2024). Facies variability and depositional cyclicity in central Northern Switzerland: Insights from new Opalinus Clay drill cores. *Swiss Journal of Geosciences*, *117*(1), 18. https://doi.org/10.1186/s00015-024-00463-6